ISSN No:-2456-2165 https://doi.org/10.38124/ijisrt/26aug308

Design and Analysis of Surface-Mounted Pm Generator for Renewable Power Generation

Amoasi Eugene[1]

[1]University of Nottingham

Publication Date: 2026/08/14

How to Cite: Amoasi Eugene (2026) Design and Analysis of Surface-Mounted Pm Generator for Renewable Power Generation. *International Journal of Innovative Science and Research Technology*, 11(8), 436-488. https://doi.org/10.38124/ijisrt/26aug308

ISSN No:-2456-2165 https://doi.org/10.38124/ijisrt/26aug308

ABSTRACT

Global concerns about climate change have brought significant attention to the generation of electricity from renewable energy sources. Wind turbine technology has gained prominent attention in renewable power generation due to its advantages over other renewable energy sources. In generating electricity from the wind using a wind turbine, one important component is the wind turbine generator. Over the years, several different types of wind generators have been designed. But one thing stands out, since the wind speed, which mainly causes the rotational energy of the turbine blades, could sometimes change with time, the energy input to the generator can equally change with time, but the generator must produce high power output and operate at the best performance. The use of a brushless permanent generator is capable of achieving this. In this thesis, an analytical approach and Finite Element Analysis (FEA) technique are introduced for the design of a high-efficiency surfacemounted permanent magnet synchronous generator. This generator is intended for use in a wind turbine that will supply power to a food manufacturing company. The designed 24 slots, 4-pole surface-mounted permanent magnet generator is capable of producing 142kW at a rated speed of 1500rpm. The Finite Element Analysis model is created based on the analytical design method. Structure optimization involves stator tooth width, slot width, number of turns, magnet arc, and magnet size, which are analyzed and simulated using ANSYS MOTOR CAD Software. The design is tested in both no-load conditions and loading conditions. In no-load conditions, the design shows a maximum cogging torque of 65Nm. In loading conditions, the generator is 98.52% efficient. Thermal analysis is carried out, and the generator's enclosure is formulated. The generator generates a temperature of 81.3 ${}^{\circ}$C in its armature windings, which represents the maximum steady-state temperature considering all parts of the machine. The ambient temperature for the designed generator to produce this temperature is 25 ${}^{\circ}$C.

ISSN No:-2456-2165 https://doi.org/10.38124/ijisrt/26aug308

TABLE OF CONTENTS

ISSN No:-2456-2165 https://doi.org/10.38124/ijisrt/26aug308

CHAPTER ONE
INTRODUCTION

➢ *Background of Study*

The many current happenings in our environment today are clear evidence of climate change. Extreme weather events such as heat waves, rising sea levels, acidification leading to the disappearance of many species, the disruption of carbon sinks, the gradual disappearance of many resources, and the fall in agricultural yields are all indications of evidence of climate change.[1] Excessive levels of greenhouse gas concentration in the Earth's atmosphere are the major cause of climate change.[2] These gases mostly come from the burning of fossil fuel-based energy sources such as coal, natural gas, and petroleum, largely for generating electricity and heat, which contribute to a larger chunk of global emissions[1].

To contribute to the reduction of the burning of fossil fuel energy sources to produce electricity, alternative energy sources are to be utilized. Renewable sources of energy, such as wind, solar, hydropower, biomass, tidal, and geothermal, have gained prominent attention in recent years due to their seeming solution to this problem. To generate electricity from renewable energy sources, a very important parameter, such as resource availability, needs to be considered. These resources are usually abundant in certain geographical areas, hence making it economically unfriendly to install renewable energy technology in all areas of the world. For instance, geothermal energy, which obtains its resource, i.e., heat from the earth's crust, is location dependent. Which is to say that it is not available at all locations. A similar analogy can be made for tidal and hydropower energy in the sense that not all countries have oceans, and not all river bodies have the potential of generating hydropower.

On the other hand, the use of biomass as a source of producing electricity comes with advantages and disadvantages. It can be argued that the burning of bioenergy sources such as wood is not intermittent or variable, unlike other sources of renewable energy, such as solar and wind, since the sun is not always shining, and the wind is not always blowing. However, depending on wood to generate electricity has the potency of causing deforestation due to unsustainable bioenergy practices. Again, apart from the upfront costs to get the plants up and running, there are additional costs associated with extracting, transporting, and storing biomass before electricity generation. These costs are absent from other renewable energy sources such as solar and wind since they rely on free on-site resources. Some of these reasons make solar and wind energy technologies highly prioritized as compared to other sources of renewable electricity.

However, solar energy has a few advantages that make it a choice over wind energy generation. In the same vein, its disadvantages make wind energy extraction suitable for renewable electricity generation. For instance, comparing wind and solar energy in terms of cost, a 10kW photovoltaic system will have an average annual production of 14,165kWh and an average cost of approximately $24,900 before tax credit [3]**.** Similarly, a 10kWh wind turbine can generate an average annual production of 14,016kWh and small-scale residential wind turbines can cost up to $75,000 before tax credits **[**3**].** Additionally, unlike solar panels, wind turbines have moving parts that could cause wear and tear, resulting in more maintenance costs after an initial investment. When comparing solar farms versus wind farms based on the numbers above, solar energy comes out ahead as a cheaper way to generate electricity for residential use.

Notwithstanding, on a utility scale such as an industrial application or grid connection, it is more efficient and cost-effective to generate electricity from wind turbines than from solar energy. This is based on the conversion efficiencies of the two technologies. For instance, the most efficient solar panel on the market can convert 20% of energy harnessed from the sun, while wind turbines can convert between 60% - 90% of the energy they harness from the wind [3]. Subsequently, wind turbines can generate electricity throughout the day, whereas solar energy can generate electricity only when the sun shines. One wind turbine can generate the same amount of electricity in kWh compared to thousands of solar panels. This implies that wind turbines will require less space to produce the same amount of electricity as solar panels. Wind farmlands can be used to grow crops, whereas solar farms, apart from requiring large installation areas, cannot be used for anything else. Considering the numerous advantages that come with generating electricity from the wind, especially with its high electricity yield, it makes wind energy the preferred choice for industrial applications and large-scale utility projects.

➢ *Problem Statement*

The wind is the primary resource in wind power generation. The wind speed, which mainly causes the rotation of the wind turbine blades, can sometimes change with time; hence, the mechanical energy input to the wind turbine's generator can equally change with time.

However, the generator must produce high-power output and operate at the best performance. A good way of achieving this is by using an electrical generator made up of a brushless permanent magnet.

➢ *Aim and Objectives*

The main aim of this research work is to design, analyze, and optimize a brushless permanent magnet generator for a wind turbine application for an off-grid food manufacturing company in Ghana. In doing this, some specific objectives to achieve are

ISSN No:-2456-2165 https://doi.org/10.38124/ijisrt/26aug308

stated as follows:

- To develop a specification of a food manufacturing industry to determine the power for which the wind turbine(s) need to be sized.
- To determine whether multiple or single wind turbines is/are required for the food manufacturing company.
- To size a wind turbine considering its swept area, height, etc. of the wind turbine blades.
- To size an electrical machine required to meet the power specifications of the food manufacturing industry.
- To perform a detailed design of a brushless electrical generator using a permanent magnet.
- To develop a MATLAB script for the machine design.
- To perform a finite element validation of the developed electrical machine.
- To perform a robustness study and sensitivity analysis of the electrical machine designed.

➢ *Justification*

CH Global Food Limited consumes an average of 297.86MWh of electricity annually, which represents $26,807.57. The cost of electricity annually represents 70% of the production cost of the factory. Wind energy for the factory will ensure that the company generates and benefits from a clean and affordable source of electricity throughout the year. This will reduce the cost of production, thereby resulting in the company's ability to produce the most affordable food products for the country and the world at large. Additionally, CH Global will have access to reliable sources of electricity without power outages, ensuring that the production target of the company is met every year. Considering the abundance of wind resources with an average wind speed of 7.05m/s at a height of 40m in the location of the factory, wind power generation will be a prudent investment for the company. The use of permanent magnets in wind turbine generators has many advantages compared to electromagnets. They can resist heating much more efficiently than electromagnets and thus require fewer cooling systems for noise pollution control, such as fans or water-cooled coils [4]. Additionally, they are also able to withstand a lot more electric current and shock than electromagnets, so they can be used in applications that generate huge currents like highvoltage electric transmission systems with no risk of heating damage [4]. Permanent magnet wind turbine generators have a much higher energy density than electric coils [4].

➢ *Background to Energy Consumption Review of CH Global Limited*

CH Global Food Limited is a cassava processing factory located in Addo Nkwanta in the Krachi East District of the Oti Region of Ghana. It has a geographical coordinate of 7°40′ 30 .7″ N 0˚19′ 26.9″E and 149m elevation above sea level. A review of the energy consumption of the factory is carried out. This is done by considering the various stages of the production processes for the cassava to gari production line. Each piece of equipment in the production process and its power rating, as well as its operating hours, are considered. Also, an energy audit process is carried out by taking into consideration the various electrical appliances in all the offices of the factory and outside the factory. The factory runs a continuous 8-hour production time, which begins at 8 am and ends at 5 pm every working day within the week, with an hour break at midday. However, the administration offices run from 7 am to 6 pm with an hour's break at midday. The production hall has all the machinery used in the cassava to gari processing.

➢ *Energy Consumption for Cassava to Gari Processing Plant*

Cassava-Gari, a dried coarse flour that undergoes fermentation and gelatinization, is widely consumed in West Africa and serves as a staple in countries such as Nigeria, Ghana, Benin, and Togo. Its growing urban popularity in West and Central Africa can be attributed to its favorable storage characteristics and its recognition as a convenient food option. Gari processing entails a series of separate operations. In this process, each stage of the Gari processing equipment is considered, and its respective power rating is noted. An average hour of use of these pieces of equipment is considered to determine the total electricity consumption for this production line. Table 1 below provides an overview of all the machinery used for cassava to gari processing. It gives a description of what the machine is used for in the production process, its power rating, and the average hours used during production.

Table 1 Description of Various Machinery in the Cassava to Gari Processing Plant.

EQUIPMENT/ PROCESS $N\bar{o}$.	IMAGE OF EQUIPMENT	BRIEF DESCRIPTION
WASHING STAGE OF CASSAVA PROCESSING		
1. Scraper Conveyor		It is constructed of carbon steel. Its purpose is to lift and convey the cassava roots to the feeding port of the cassava washing machine. It has a rated power of 2.2kW. During production days, It is estimated to operate for 8 hours of production periods.

ISSN No:-2456-2165 https://doi.org/10.38124/ijisrt/26aug308

2. Horizontal Cage Type Cleaner		It is constructed with carbon steel. Its purpose is to wash the cassava roots without water to remove stains and dirt. It has a power rating of 2.2kW, and it operates for an average time of 8 hours.
3. Paddle Type Cleaner		It is made of carbon steel. It washes the cassava roots in clean water to remove stains and dirt. It has a power rating of 3.0kW. It operates for an average o f 8 h o u r s during production hours.
4. Cassava Peeling Machine		This machine is constructed of stainless steel. It is used to wash the cassava roots to remove the outer brown skin and the partial inner thick cream layer. It is rated 3.0kW. During production days, it operates for an average of 8 hours.
5. Inspection Table Conveyor	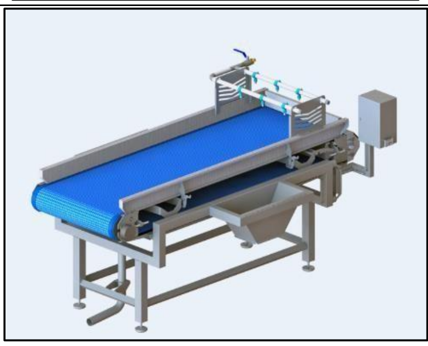	This machine is constructed using stainless steel. It links the cassava peeling machine to the grinding machine while serving as a platform for the inspection of peeled cassava roots. It is rated 1.5kW and operates during the entire 8 hours of production days.
EXTRACTION STAGE OF CASSAVA PROCESSING		
6. Cassava Grinding Machine		It is made of stainless steel. Its purpose is to crush the washed cassava roots into a uniform paste or mash. It has a power rating of 15kW, and it operates for an average of 8 hours during production days.

ISSN No:-2456-2165 https://doi.org/10.38124/ijisrt/26aug308

7. Mash Pump Machine		They are made of stainless-steel material, which links the grinding machine to the hydraulic press dewater by pumping the cassava mash generated by the grinding machine. For one production line, there are two sets of them. Each is rated 2.2kW and works 8 hours during production days.
8. Hydraulic Press Dewater		They are made of stainless steel. In one production line, there are four sets of them. They press the cassava mash to remove as much moisture as possible. Each is rated 4kW and operates 8 hours continuously during production days.
9. Wet Cake Crusher Machine		It is made of stainless steel. It crashes and presses wet cake into particles of uniform size. It has a power rating of 5.5kW and will operate for 8 hours during production days.
10. The Conveyor Machine		It is constructed with carbon steel material. It links the hydraulic press dewater and the wet cake crusher by lifting and conveying the pressed cakes to the feeding port of the cake crusher. It has a rated power of 1.5kW a n d operates for an average of 8 hours per production day.

ISSN No:-2456-2165 https://doi.org/10.38124/ijisrt/26aug308

11. The Screw Conveyor		This is made up of a stainlesssteel material that conveys the dewatered wet gari particles to the gari flying machine. It has a rated power of 1.5kW and is expected to work for an average of 8 hours during production days.
GARI FORMATION STAGE OF CASSAVA PROCESSING		
12. Gari Milling Machine		It is constructed from stainless steel material and has a rated power of 22kW. It is used for milling coarse gari granules into fine granules with uniform sizes and operates for 3 hours.
13. Gari Frying Machine		These machines are made up of stainless steel. For one production line, there are five sets of them. Each is rated 1.5kW. They are meant for roasting the gari granules in a hot frying tray or pan to form the final dry and crispy product. It operates at an average of 10 hours during production hours.
14. Screw Conveyor Machine	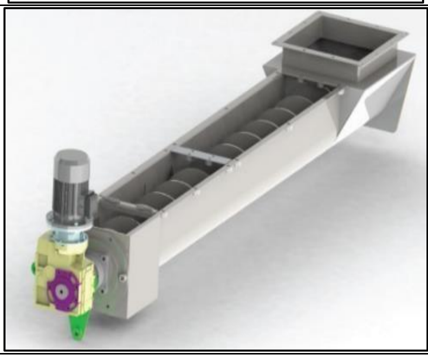	It is made of stainless steel, which links the gari frying machine and cyclone unit. It conveys the fried gari to the feeding port of the cyclone unit. It has a power rating of 3.0kW. It operates for an average of 8 hours during production periods within the day.
15. The Cyclone Dust Collecting and Induced Draft Fan Machine	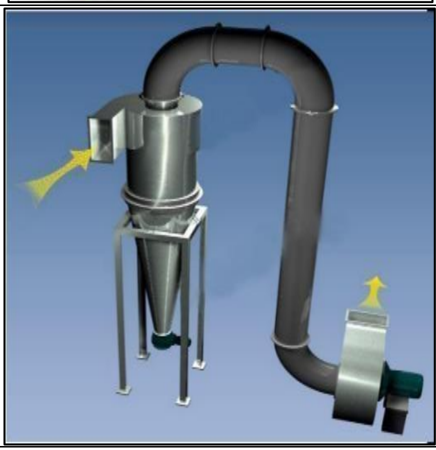	It is constructed of stainless steel, which has a power rating of 5.5kW. It absorbs the dry gari into the sieving machine by the principle of negative pressure and dust collecting. Averagely, it operates for 8 hours.

ISSN No:-2456-2165 https://doi.org/10.38124/ijisrt/26aug308

16. Gari Sieving Machine	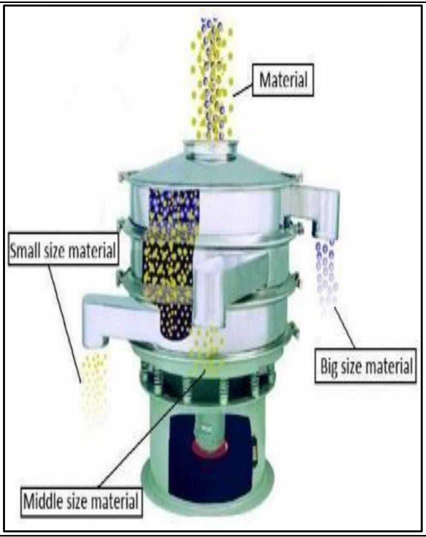	It is constructed with food contact stainless steel, which is meant for sieving the coarse gari granules to separate from the fine granules. It has a power rating of 0.75kW, and it operates for an average of 8 hours.
17. The Lifting Machine		It is a stainless-steel constructed machine that lifts and conveys the gari particles to the packaging machine. It has a power rating of 1.5kW and operates for 8 hours during production hours.
18. The Standard Big Bag Packaging Machine.		It is constructed with carbon steel. It has a power rating of 3.0kW and its purpose is to pack desired quantities of dried gari into a woven polythene sack with a plastic lining, seal or stitch the sack. Its operating hours are approximately 3 hours of production time. Depending on the customer's specification
		This machine is used or unused. The other type of this machine is the small bag packaging machine, which is rated at 2.2kW and has average operating hours of 5 hours during production, mainly operated depending on the product to be supplied.

ISSN No:-2456-2165 https://doi.org/10.38124/ijisrt/26aug308

19. Screw Auger Feeding Machine		It is constructed with stainless steel and has a power rating of 1.5kW. Its purpose is to lift and convey the coarse gari particles to the feeding port of the milling machine. This part of the equipment process is not usually used unless there is a specification from a customer. On average, it is estimated to be used for only 3 hours.
20. Gari Milling Machine		It is constructed from stainless steel material and has a rated power of 22kW. It is used for milling coarse gari granules into fine granules with uniform sizes and operates for 3 hours.

ISSN No:-2456-2165 https://doi.org/10.38124/ijisrt/26aug308

CHAPTER TWO
LITERATURE REVIEW

➢ *Different Types and Configurations of Wind Turbines*

In general, wind turbine design can be classified into two categories, namely, Horizontal Axis Wind Turbines (HAWTs) and Vertical Axis Wind Turbines (VAWTs).

- *Vertical Axis Wind Turbines (VAWTs):*

This wind turbine design features a main rotor shaft positioned perpendicular to the wind, with the primary components situated at the turbine's foundation. There are generally two types of wind turbines, the Savnoius and the Darrieus [7].

Fig 1 The Different Types of Vertical Axis Wind Turbine, the Savnoius and Darrieus Respectively.[8]

They function closer to the ground and have the advantage of making it possible to have heavy equipment, such as the gearbox and generator, close to the ground instead of the nacelle, as in the case of HAWT. However, at the ground level, the wind speed is lower and mostly affected by the terrain, thereby leading to less power generated. VAWT does not require a yaw mechanism, since it can harness the wind from all directions as compared to HAWT, and this is one advantage over HAWT. Unfortunately, this advantage is limited by factors such as time-varying power output because of the change of power in single-blade rotation, the requirement for guy wires to support the main tower, and the fact that Darrieus VAWTs are not self-starting, unlike HAWT. [7]. Notwithstanding, VAWT gives many advantages when compared to traditional horizontal-axis wind turbines. They may be packed very close together inside the wind farms and this allows more in any space. They are also quiet when operating, omnidirectional, and generate lower forces on the support structure. They also do not need much wind to produce power, therefore permitting them to be nearer to the ground where the speed of the wind is lower. Due to their closeness to the ground, it is easier to carry out maintenance on them. Additionally, they can be implemented on tall structures. [7]. The use of VAWTs has disadvantages as well. They generate extremely low starting torques and have dynamic stability issues. [7]. They also do not function properly under gusty winds. [7]. The blades that are attached to HAWT are vulnerable to types of fatigue because of the broad variation in applied forces with every rotation. The vertical types of blades implemented in early models became bent with every spin, and this caused them to have cracks. With time, the blades broke, and this led to failure of the turbine. This makes VAWTs less reliable.[8].

- *Horizontal Axis Wind Turbine (HAWTs):*

It is a type of wind turbine in which the shaft of the rotor is in the direction of the wind and the main components are in the nacelle on top of the tower. It is the most common model for drawing energy from the wind and offers a great number of advantages. For HAWT to have maximum efficiency, they must point in the right direction, i.e., into the wind or away from the wind, based on the type. [7]. Those that are positioned away from the wind are called downwind turbines, and those positioned toward the wind are

ISSN No:-2456-2165 https://doi.org/10.38124/ijisrt/26aug308

called upwind turbines. [7]. In traditional and smaller upwind turbines, precise alignment is achieved with the assistance of a basic wind vane. In contrast, larger turbines employ a yaw motor and yaw meter system. The yaw meter detects the exact wind direction, and the yaw motor reorients the turbine to constantly face the wind. There are several advantages to using HAWTs. Firstly, the variable pitch of the blades used for a horizontal wind turbine allows it to collect the maximum amount of energy from the wind. Since the blades of HAWT are perpendicular to the direction of wind, it receives more power from the wind for rotation. HAWTs are popular options for wind energy generation, both for home and hybrid systems applications.

Fig 2 An Image of a Horizontal Axis Wind Turbine [8]

Being the dominant wind turbine model for decades, research and development of it are already at the mature stage. Not only do current products available in the market demonstrate reliability, but there is also an extensive exploration of the application and utilization of horizontal-axis wind turbines. The taller tower height of horizontal-axis wind turbines allows them to harness higher wind speeds, as wind velocity typically rises with greater elevation [8]. Also, the airflow at such height is relatively stable, horizontal axis wind turbines enjoy more consistency in wind and thus in power output.

- *Conclusion:*

Horizontal Axis and Vertical Axis Wind Turbines have been discussed above. Due to the numerous advantages of HAWTs over VAWT, HAWTs are widely used in both commercial and domestic wind power generation.

➢ *Components of Horizontal Axis Wind Turbine*

A wind turbine works on a simple principle; instead of using electricity to make wind, as in the case of fans, wind turbines use wind to make electricity. They convert kinetic energy from the wind into electrical power. Before this conversion can take place, it has several components to aid the process. Modern wind turbines have many different parts, which can be broken down into three major components: the tower, nacelle, and rotor blade.

- *The Tower:*

It carries the nacelle and the rotor. Towers for large wind turbines may be either tubular steel towers, lattice towers, or concrete towers. The tower also provides a channel through which electrical cables are laid from the generator to the point of grid connection. Also, it serves as a channel to reach the nacelle for any maintenance work. In the construction of the tower, it must be tall enough to ensure the rotor blades do not interfere with normal day-to-day operations at ground level. Again, to ensure the tower is securely attached to the ground, for example, a 2MW onshore wind turbine would first require a 15- to 20-foot-deep concrete foundation

ISSN No:-2456-2165 https://doi.org/10.38124/ijisrt/26aug308

pad, poured, requiring approximately 30,000 tons of concrete [8]. The anchor bolts for the tower are then embedded deep into the concrete pad itself. The base of the tower will then be securely bolted onto the concrete foundation pad. The tower must be strong enough to hold up the nacelle and the rotor throughout all weather conditions. For a 2MW onshore wind turbine, the weight of the steel support pillar alone can be 220 tons [8].

- *The Rotor Blades:*

The rotor blades are usually three long, thin blades that attach to the hub of the nacelle. Blades are constructed of a composite of wood, fiberglass, resin, and carbon. These structures can have as many as 102 layers of materials in the root ends and as few as two at the tips. As is the case with most wind turbine components, the design and build quality of the blade are critical because tip speeds commonly exceed 160 miles per hour during operation. When wind flows across the blades, the air pressure on one side of the blades decreases. The difference in air pressure across the two sides of the blade creates both lift and drag forces. The force of the lift is stronger than the drag force, and this causes the rotor to spin. The rotor shaft connects to the generator either directly or through a gearbox that increases the speed of rotation of the mechanical input to the generator. The conversion of aerodynamic forces to the rotation of a generator creates electricity.

- *The Nacelle:*

It is always mounted on top of the support tower. The rotor blade assembly is attached to the front of the nacelle. Like wind turbine blades, nacelles are typically very large parts made of composite plastics over a light wood core. They must be able to withstand high mechanical stress without degradation, which leads to inefficient power generation. The nacelle houses some essential components needed for power conversion. The gearbox assembly, aerodynamic braking system, mechanical braking system, turbine generator, and electrical power transmission systems are all located in the nacelle [8].

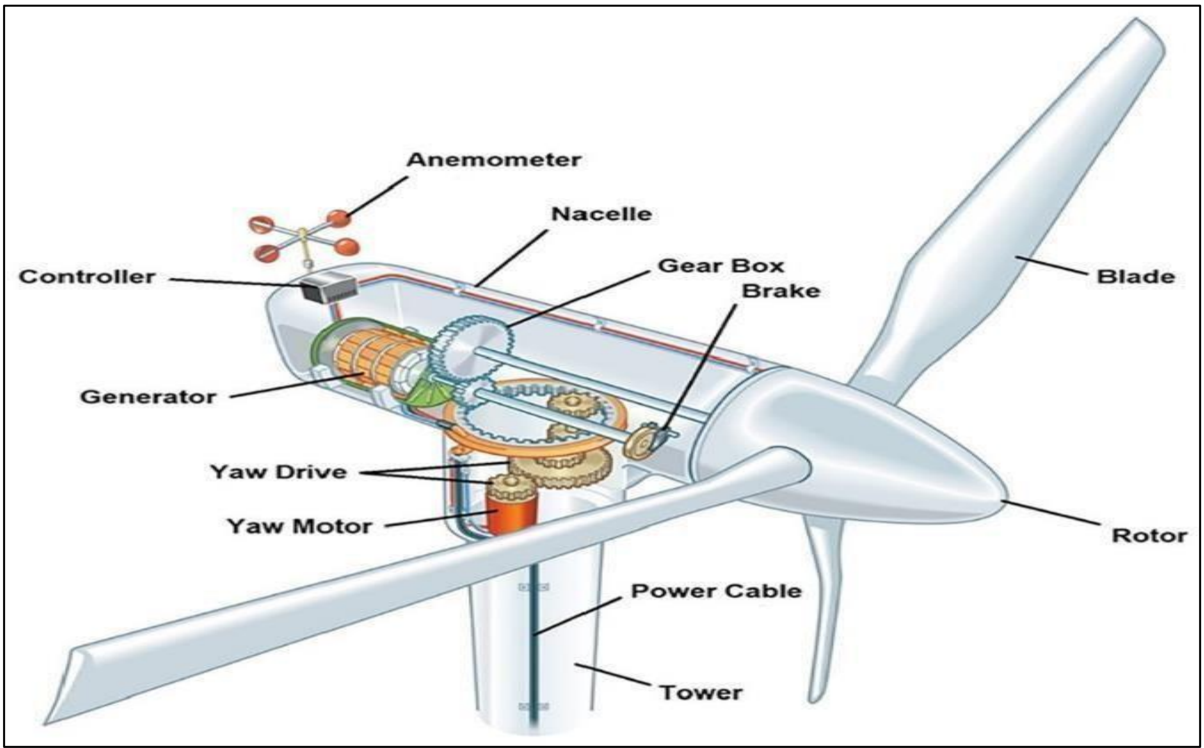

Fig 3 Components Contained in the Nacelle of a Wind Turbine Obtained from Journals.Sagepub.Com [8]

- *The Gearbox Assembly:*

The gearbox assembly is mostly used in a gearbox wind turbine. For direct-drive wind turbines, gearboxes are not applicable. The purpose of the gearbox assembly is to receive the rotating input shaft from the center of the rotor blade assembly using a system of gears. The gears speed up the rotation to a high speed suitable for running the turbine generator at the required generation speed.

- *Aerodynamic Braking:*

When the wind speed becomes more than required, or the rotation of the rotor shaft needs to be stopped for maintenance works or to reduce the generation of electric power on the grid, modern wind turbines are designed to have two braking systems. The Aerodynamic braking is achieved by twisting the rotor blades, so they present a thinner cross-section to the oncoming wind. This will mean that the rotor blades will rotate more slowly. On the other hand, mechanical braking, which is usually incorporated into the gearbox assembly, has a rotating disk mounted onto the input shaft of the gearbox, and using a hydraulic actuator, brake pads are clamped onto the disc, thus gradually slowing the gearbox assembly to a complete stop. In the case of high wind speeds exceeding

ISSN No:-2456-2165 https://doi.org/10.38124/ijisrt/26aug308

the required speed, the rotational speed of the blades is controlled by using aerodynamic braking alone. Mechanical braking is only deployed if the turbine needs to be stopped completely.

- *The Electrical Power Transmission System:*

Since the emF generated by the rotating magnetic field depends on the speed of the rotor, which is sometimes variable due to the variability of the wind, power converters are used to convert the generated emf into a required grid voltage and frequency.

➢ *Understanding Wind Power Generation*

Whenever an object of a given mass is in motion with a translational or rotational speed, Kinetic energy is said to exist. Similarly, when air is in motion, the kinetic energy contained in the air could be determined as,

$$E_K = \frac{1}{2} m\bar{u}^2 \tag{1}$$

Where m = mass of the air and $\bar{u}$ = is the mean wind speed over a suitable time.

The power contained in the wind is obtained by differentiating the kinetic energy with time.

$$P_w = \frac{dE_k}{dt} = \frac{1}{2} \dot{m}\bar{u}^2 \tag{2}$$

When wind passes through a wind turbine and rotates the blade, the resultant wind mass flow rate is given as,

$$\dot{m} = \rho A\bar{u} \tag{3}$$

$$P_w = \frac{1}{2} \rho A\bar{u}^3 \tag{4}$$

By examining equation 5, it is evident that the wind power is directly dependent on the swept area of the wind turbine, the density of the wind, and the cubic power of the mean wind speed. This means that making the blades of the wind turbine longer results in a higher swept area and higher air density capture. This will result in a higher power capture by the wind turbine. The cubic power relationship between the wind power and the mean wind speed signifies that a small change in the wind speed can result in a large change in wind power.

The aerodynamic power contained in the wind is therefore given by the relation, $P_w = \frac{1}{2} \rho A\bar{u}^3$ where, $\rho = 1.225 kg/m^3$ $\bar{u}$ = average wind speed and A=swept area of the wind turbine's blade However, not all the power captured by the wind turbine is converted into mechanical energy.

The power coefficient (C_p) established by Betz's Law states that only a theoretical maximum value of 59.3% of the aerodynamic power captured by the wind turbine can be converted into mechanical energy [5]. Additionally, real wind turbines do not reach this theoretical optimum, good systems have power co-efficient between 0.4 – and 0.5[9]. From this, the mechanical power generated by a wind turbine is expressed mathematically as.

$$P_{mech} = \frac{1}{2} \rho A\bar{u}^3 c_p \tag{5}$$

Wind turbines can be gearing-driven or direct-driven. In recent years many wind farm failures have been attributed to failures of gearbox systems. This has resulted in the increasing focus on direct-drive wind turbines. However, since the wind speed can be low, direct-drive wind turbine generators tend to have larger diameters due to the high number of poles required. On the other hand, gearbox-driven types of wind turbine generators allow for a smaller number of poles, resulting in a smaller generator diameter. It also allows generators to run at high speed. It is advantageous to use a gearbox-driven type of wind turbine, especially for onshore applications where maintenance can easily be carried out. In wind turbine applications where a gearbox is employed, the mechanical input power to the generator is expressed mathematically as.

ISSN No:-2456-2165 https://doi.org/10.38124/ijisrt/26aug308

$$P_{mech} = \frac{1}{2}\rho A\bar{u}^3\, c_p\, \boldsymbol{\eta}_{GB} \tag{6}$$

Where $\boldsymbol{\eta}_{GB}$ is the efficiency of the gearbox. Since the gearbox is not 100% efficient, some amount of mechanical power generated by the wind turbine is lost through the gearbox.

Subsequently, the remaining mechanical energy is what rotates the generator's rotor to generate electrical power. However, wind turbine generators are not 100% efficient. Hence, some amount of energy is lost in the conversion process. Additionally, power electronic devices are used to convert the power generated by the wind turbine's generator into a fixed frequency and voltage power output. Since it is not 100% efficient, its efficiency will affect the electrical power produced by the turbine. Hence, the mathematical expression for calculating the electrical power from a wind turbine, considering all losses, is given as.

$$P_E = \frac{1}{2}\rho A\bar{u}^3\, c_P \eta_{GB}\eta_G\eta_P \tag{7}$$

Where ηG is the generator efficiency, and ηP is the efficiency of the power converters.

➢ *Wind Turbine Generators*

The generator is the component that turns the rotational energy in the high-speed output shaft from the gearbox or the rotor assembly shaft, as in the case of direct-drive turbines, into an electrical current. The rotor of the generator is usually made up of a permanent magnet or electromagnet, which is usually magnetized when connected to a DC source. As the rotor rotates, an EMF is induced in the stator wires. One of the key factors limiting wind turbines is their generator technology. There is no consensus among academics and industry experts regarding the optimal wind turbine generator technology. Traditionally, three primary types of wind turbine generators (WTGs) have been considered for various wind turbine systems: they are direct current (DC), alternating current (AC) synchronous, and alternating current asynchronous generators.[10] Each of these can be operated at either fixed or variable speed. Utilizing variable speed for WTGs is beneficial due to the fluctuating nature of the wind power. This approach reduces physical stress on the turbine blades and drive trains, while also improving system aerodynamic efficiency and torque transient behaviors. [10].

- *Alternating Current Synchronous Generators:*

AC synchronous WTGs can be driven by DC excitations of wound rotors or using either permanent magnets, popularly referred to as PMSGs - Permanent Magnet Synchronous Generators, or electromagnets, also referred to as EESGs - Electrically Excited Synchronous Generators. When the wind turbine's rotor is in motion, the stator windings generate a three-phase power output connected to the grid through transformers and power converters.

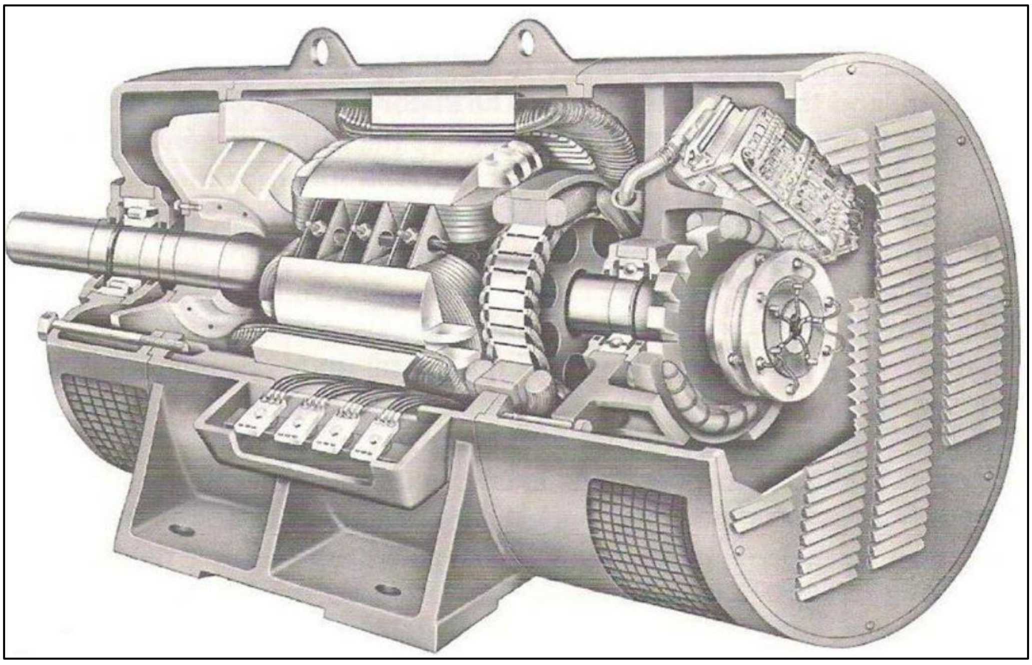

Fig 4 Figure 2.8: Cutaway of a Synchronous Generator [10]

ISSN No:-2456-2165 https://doi.org/10.38124/ijisrt/26aug308

For fixed-speed synchronous generators, maintaining the rotor speed exactly at the synchronous speed is essential to avoid loss of synchronism. In recent years, there has been a gradual adoption of PM generators in wind turbine applications due to their high-power density and lightweight construction. These generators are favored for small power capacity wind turbine generators. The generator's structure is relatively simple, with rugged PMs placed on the rotor to create a constant magnetic field, and electricity is generated in the armature (stator) using commutators, slip rings, or brushless. In some cases, PMs can be incorporated into a cylindrical cast aluminum rotor to reduce costs. The operational principle of PM generators resembles that of synchronous generators, except that PM generators can function asynchronously. PMSGs offer various advantages, such as the elimination of commutators, slip rings, and brushes, resulting in rugged, reliable, and straightforward machines. The use of PMs removes the need for field windings and associated power losses, but it also makes field control impossible, and the cost of PMs can be prohibitive for large machines. Due to the varying wind speeds, PMSGs are unable to produce electrical power at a constant frequency. Consequently, they need to be linked to the power grid using AC-DCAC conversion facilitated by power converters. This entails transforming the generated AC power (which exhibits fluctuating frequency and magnitude) into steady DC power, followed by its reconversion into AC power with consistent frequency and magnitude. Utilizing these permanent magnet machines for direct drive applications is also highly appealing. In such scenarios, they can eliminate problematic gearboxes, which are a primary source of wind turbine malfunctions. These machines require a greater number of poles and possess larger physical dimensions compared to equivalently rated geared machines.

ISSN No:-2456-2165 https://doi.org/10.38124/ijisrt/26aug308

CHAPTER THREE
POWER CALCULATION AND SPECIFICATION OF CH GLOBAL FOOD LIMITED

➢ *Summary of Energy Consumption of the Factory*

As discussed in Chapter One above, the table below provides a summary of all machinery in the cassava to gari processing line, which indicates their power rating, average operating hours, and total electricity consumed during production hours.

Table 2 Summary of Energy Consumption of the Cassava to Gari Processing Plant.

Name of Equipment	Power Rating (kW)	Average Operation Hours	Energy Consumed (kWh)
1. Scraper Conveyor	2.2	8	17.6
2. Horizontal Cage Type Cleaner	2.2	8	17.6
3. Paddle Type Cleaner	3.0	8	24.0
4. Cassava Peeling Machine	3.0	8	24.0
5. Inspection Table Conveyor	1.5	8	12.0
6. Cassava Grinding Machine	15	8	120
7. Mash Pump Machine	4.4	8	35.2
8. Hydraulic Press Dewater	16	8	128
9. The Conveyor Machine	1.5	8	12.0
10. Wet Cake Crusher Machine	5.5	8	44.0
11. The Screw Conveyor	1.5	8	12.0
12. Gari Frying Machine	7.5	10	75.0
13. Screw Conveyor Machine	3.0	8	24.0
14. Cyclone Dust Collecting	5.5	8	44.0
15. Gari Sieving Machine	0.75	8	6.00
16. The Lifting Machine	1.5	8	12.0
17. The Standard Big Bag Packaging	2.2	5	11.0
18. Screw Auger Feeding Machine	1.5	3	4.50
19. Gari Milling Machine	22	3	66.0
TOTAL	99.75		688.90

➢ *Energy Consumption of the Factory's Building*

Apart from the cassava to gari processing plants that contribute to the major consumption of electricity in the factory, electrical gadgets in the various offices of the factory also contribute to its total electricity usage. A load assessment is carried out of these facilities to estimate their contribution to electricity consumption. The factory has one production hall which is 45 meters in length, 12 meters in width, and 7 meters in height. Additionally, there are four other offices, namely the engineering office/store, staff block, guest/conference room, workers' changing room, and general manager's office. Electrical gadgets in these offices are assessed by considering their power rating, quantity, and hours of usage.

Table 3 A summary of the Building Energy Load Assessment.

Location	Electrical Appliance	Quantity	Power Rating (W)	Total Wattage (W)	Operating Hours (h)	Energy Consumed (kWh)
Production floor	LED Bulbs	40	36	1440	8	11.52
	Smoke Detectors	10	6	60	24	1.44
Engineering Office/Store	LED Bulbs	3	36	108	8	0.86
	42In. Television	1	52	52	8	0.42
	Refrigerator	1	100	100	24	2.40
	Desk. Computer	2	200	400	8	3.20
	Air Conditioner	1	2000	2000	8	16.0
	Smoke detector	2	6	12	24	0.29
Staff Block	Photocopier	1	800	800	8	6.40
	Television	1	52	52	8	0.42
	Refrigerator	1	100	100	24	2.40
	Desk. Computer	6	200	1200	8	9.60
	Air conditioner	2	2000	4000	8	32.0
	Smoke detector	3	6	18	24	0.43
General Manager's	Television	1	52	52	8	0.42
	Air conditioner	1	2000	2000	8	16.0
	Desk. Computer	1	200	200	8	1.60

ISSN No:-2456-2165 https://doi.org/10.38124/ijisrt/26aug308

Office	Canon Printer	1	50	50	8	0.40
	Refrigerator	1	100	100	24	2.40
	Smoke detector	1	6	6	24	0.14
Guest/Conferene Room	Air conditioner	1	2000	2000	8	16.0
	Monitor Screen	1	52	52	3	0.16
	Smoke Detector	1	6	6	24	0.14
Security Lights & Security Reception	Floodlights	8	50	400	12	4.80
	LED Bulbs	2	36	72	8	0.58
	Smoke Detector	1	6	6	24	0.14
TOTAL				**15286**		**130.16**

From Tables 3 and 2 above, the total energy consumption of the factory is calculated as,

Daily Energy Required = Daily Building Load Energy + Daily Gari Processing Load Energy

= 130.16 + 688.90

= 816.06kWh

Average Annual Energy Consumption = Daily Energy Required * 365 days

= 816.06kWh * 365 days

= 297.86MWh

Peak Power Required = Building Load Power Required + Gari Processing Plant Power.

= 15.286 + 99.75

= 115.036kW

ISSN No:-2456-2165 https://doi.org/10.38124/ijisrt/26aug308

CHAPTER FOUR
WIND TURBINE DESIGN

➢ *Wind Resource Assessment of Addo Nkwanta in the Krachi East District of Ghana*

One of the primary resources required for wind power generation is wind resource assessment. Wind resource assessment is the process of estimating how much wind will be available for a wind power plant throughout its useful life. It helps to predict the availability and the characteristics of the wind available at a particular location. The outcome of this assessment determines whether a particular location is suitable for wind power generation. In this assessment, a large wind dataset comprising the monthly average wind speed of 41 years was obtained from NASA's website (https://power.larc.nasa.gov/data-access-viewer/) for the location of the factory with geographical coordinates 7 4̊0′ 30 .7″ N 0˚19′ 26.9″E. The average of each year was obtained, and a subsequent average of the years representing the average wind speed of the location was established. The wind speed data was obtained at a height of 10m. The table below shows the monthly average wind speed for the years from 1981 to 2021.

Table 4 Average Wind Speed Data of Addo Nkwanta in the Krachi East District of Ghana.

		WIND SPE ED DATA AT GEOGRAPHICA L COORDINATES 7 4˚0′ 30 .7 ″ N 0˚19′ 26.9″E AT A HEIGT OF 10m											
YEAR	**ANUAR**	**FEBRUARY**	**MARCH**	**APRIL**	**MAY**	**JUNE**	**JULY**	**AUGUST**	**EPTEMBE**	**OCTOBER**	**NOVEMBE**	**DECEMBER**	**ANNUAL AVG. WIND SPEED (m/s)**
1981	1.9	2.75	2.99	3.27	2.88	3.11	3.92	3.7	3.09	2.78	2.41	2.23	2.92
1982	2.51	2.8	3.05	3.28	2.93	3.2	3.52	3.99	3.13	2.9	2.14	2.12	2.97
1983	2.66	2.95	3.55	3.7	3.3	3.42	3.71	3.82	3.17	3.03	2.99	2.74	3.26
1984	2.96	3.27	3.4	3.62	2.9	2.98	3.27	3.35	3.16	2.7	2.44	2.18	3.02
1985	2.67	2.83	3.52	3.36	3.52	3.52	3.45	3.41	3.14	2.75	2.36	2.29	3.07
1986	2.31	3.2	3.12	3.61	3.34	3.09	3.61	3.27	2.78	2.84	2.38	2.09	2.97
1987	2.52	3.48	3.27	3.63	3.92	3.3	3.25	3.44	3.01	2.7	2.39	2.33	3.1
1988	2.48	3.17	3.37	3.37	3.48	3.13	3.77	3.84	3.14	2.81	2.51	2.25	3.11
1989	2.96	3.08	3.42	3.62	3.66	3.29	3.29	3.61	2.77	2.58	2.42	2.19	3.08
1990	2.65	2.86	3.19	3.42	3.35	3.38	3.66	2.9	2.64	2.76	2.93	2.68	3.03
1991	2.77	3.49	3.51	3.48	2.9	2.86	3.45	3.9	2.59	2.67	2.61	2.47	3.05
1992	2.93	2.91	3.46	3.4	3.16	3.49	3.83	3.88	3.3	2.83	2.7	2.55	3.2
1993	2.78	3.29	3.3	3.39	3.43	3.29	3.79	3.52	2.76	2.55	2.6	2.16	3.07
1994	2.52	3.19	3.46	3.73	3.27	3.34	3.6	3.89	3.61	2.48	2.16	2.73	3.16
1995	2.3	2.72	3.33	3.34	3.13	3.39	3.87	3.62	3.23	2.89	2.39	2.53	3.06
1996	2.69	3.34	3.57	3.17	3.41	3.41	3.74	3.79	3.35	2.95	2.51	2.59	3.21
1997	2.88	2.77	3.02	3.53	2.9	3.52	4.2	3.47	3.01	2.6	2.58	2.3	3.06
1998	2.68	2.94	3.16	3.57	3.36	3.02	3.53	3.61	2.94	2.94	2.92	2.69	3.12

ISSN No:-2456-2165 https://doi.org/10.38124/ijisrt/26aug308

1999	2.72	2.76	3.16	3.36	3.2	3.16	3.45	3.62	3.29	2.74	2.57	2.21	3.02
2000	2.76	2.66	2.94	3.59	3.55	3.18	3.39	3.27	3.15	2.77	3.02	2.55	3.07
2001	2.42	2.91	3.59	3.49	3.31	3.29	3.92	3.83	3.2	2.84	2.88	2.81	3.21
2002	2.61	2.93	3.58	3.41	3.21	3.36	3.48	3.55	2.99	2.9	2.61	2.68	3.11
2003	2.64	2.98	2.96	3.31	3.48	3.07	3.51	3.6	2.82	2.52	2.3	2.09	2.95
2004	2.38	2.59	2.96	3.23	3.36	3.16	3.22	3.44	2.52	2.74	2.45	2.01	2.84
2005	2.65	2.9	3.27	3.21	3.23	3.43	3.6	3.65	2.94	2.56	2.23	2.24	2.99
2006	2.55	3.09	3.19	3.2	2.94	2.76	3.58	3.79	2.95	2.67	1.98	1.97	2.89
2007	2.55	2.92	3.08	3.2	2.85	3.59	3.69	3.59	2.63	2.44	2.43	1.94	2.91
2008	2.88	2.36	3.08	3.16	2.94	3.14	3.31	3.38	2.79	2.33	2.14	2.31	2.82
2009	2.69	2.95	3.06	2.84	3.07	2.98	3.44	3.27	2.52	2.65	2.41	2.41	2.86
2010	2.59	3.04	3.09	3.32	3.09	2.95	3.63	3.45	2.89	2.61	2.45	2.2	2.95
2011	2.44	2.98	3.07	3.13	3	3.16	3.33	3.55	2.78	2.7	2.5	2.09	2.9
2012	2.53	2.96	2.89	3.12	3.09	3.02	3.5	3.54	2.73	2.52	2.5	2.13	2.88
2013	2.52	2.8	3.28	3.09	3.27	3.51	3.39	3.58	2.85	2.8	2.79	2.64	3.05
2014	2.88	3.1	3.22	3.02	2.94	2.95	3.54	3.63	2.73	2.77	2.54	2.48	2.98
2015	2.98	3.28	3.09	3.09	3.27	3.38	3.37	3.43	2.88	2.59	2.48	2.37	3.02
2016	2.8	2.75	3.2	3.31	3.34	3.37	3.32	2.99	2.39	2.34	2.23	2.16	2.85
2017	2.41	2.47	3.28	3.23	2.95	2.79	3.27	3.4	2.68	2.25	2.32	2.38	2.79
2018	2.37	3.07	3.22	3.26	3.25	3.25	3.23	3.71	2.62	2.15	1.97	2.05	2.84
2019	2.43	2.68	2.97	3.03	2.86	3.13	3.24	3.55	2.59	2.62	2.13	1.8	2.75
2020	2.33	2.38	2.95	3.2	3.01	3.15	3.73	3.84	2.95	2.48	2.11	2.23	2.86
2021	2.45	2.66	3.15	3.37	3.46	2.89	3.73	3.27	2.59	2.48	2.2	1.95	2.85
AVERAGE WIND SPEED (m/s)													3.0

- *Estimating Hub Height and Corresponding Average Wind Speed*

From Table 4 above, it is estimated that the average wind speed at 10m for the location of the factory is 3.0 m/s**.** However, ground-level obstacles such as vegetation, buildings, and topographic features tend to slow the wind near the surface. As we go above the ground, the speed of the wind increases because the effect of these obstacles decreases with increasing height above the ground [11]. This variation of wind speed with height is called wind shear. To estimate the average wind speed at the turbine's hub height, where the power curve is defined, the turbine's hub height must be known. To allow for some length of clearance of the turbine's blade from the ground level, the diameter of the wind turbine blades is usually known to be proportional to the hub height. Based on the average wind speed of the location and the expected annual energy output required, if the diameter of the wind turbine is chosen to be 40m, then the hub height should be equal to or above 40m. A mathematical model known as the power law is used to estimate the average wind speed at this height. Extrapolating NASA Earth data at 10 m wind data to a turbine hub height introduces significant wind speed bias (typically 1% to 8%) and annual energy yield uncertainty (exceeding 6% at higher levels). The power law represents a simplified model for the vertical wind speed profile using boundary layer theory and considers the surface roughness. The mathematical equation of the power law theory is given as,

$$\frac{U(z)}{U(z_r)} = \left(\frac{z}{z_r}\right)^{\alpha} \quad (8)$$

Where α is the wind shear exponent (power law exponent), for terrain, which is characterized

By forest and woodland, the roughness exponent of the terrain is given as 0.616[12].

$U(z_r)$ is the average wind speed at height z_r, 10m.

U (z) is the average wind speed at height z, 40m

$$\text{From equation 9, } U(z) = \left(\frac{z}{z_r}\right)^{\alpha} \times U(z_r)$$

$$U(z) = \left(\frac{40}{10}\right)^{0.616} \times 3m/s$$

= 7.05m/s, Hence, the average wind speed at a height of 40m is obtained as 7.05m/s.

- *Design Specification of the Proposed Wind Turbine*

In this section, the various specifications of the wind turbine are designed considering the wind resource available and the load requirement of the factory. The aerodynamic power contained in the wind is calculated as,

$$P_w = \frac{1}{2}\rho A\bar{u}^3 \quad (9)$$

Where, $\rho = 1.225kg/m^3$ $\bar{u} = 7.05m/s$ A = swept Area of wind turbine blades

$$= \frac{1}{2} \times 1.225 \times \boldsymbol{A} \times (7.05)^3$$

$$= 214.6216\mathbf{A} \quad (10)$$

Assuming the Cp of the proposed wind turbine at a rated wind speed of 7.05m/s is chosen as 0.5. Then the mechanical power of the wind turbine is calculated as,

$$P_{mech} = \frac{1}{2}\rho A\bar{u}^3 c_p \quad (11)$$

Substituting Equation 11 into Equation 12,

$= 214.6216\mathbf{A} \times 0.5$

$= 107.3108A$ (12)

The design incorporates a gearbox to increase the speed of the generator's rotor. Hence, a Gearbox efficiency is assumed.

ISSN No:-2456-2165 https://doi.org/10.38124/ijisrt/26aug308

Similarly, the generator's efficiency is assumed at this stage as well as the power converters' efficiency. Assumed gearbox efficiency (η_{GB}) = 0.93 Assumed Generator Efficiency (η_G) = 0.9 Assumed Power Converter efficiency (ηP) = 0.9 Hence, the electrical power generated by the proposed wind turbine is calculated as,

$$P_E = \frac{1}{2}\rho A\bar{u}^3 c_P \eta_{GB}\eta_G\eta_P \tag{13}$$

Substituting Equation 13 into Equation 14, $P_E = P_{mech}\,\eta GB\eta G\eta P$

= 107.3108**A** × 0.9 × 0.93 ×0.9

= 80.8372**A** W/m^2

The Electrical Power Produced by the Wind Turbine = Peak Electrical Power of the Factory

$$80.8372 \times A = 115.036 \times 10^3 \tag{14}$$

$$A = \frac{115.036 \times 10^3}{80.8372}$$

$$= \mathbf{1423.0577m^2}$$

Hence, the swept area of the wind turbine's rotor required to meet the factory's load is 1423.0577m^2. Based on this, the diameter of the wind turbine's blades is calculated as,

$$A = \frac{\pi D^2}{4}, \quad D \text{ and } A \text{ are the diameter and swept area of the rotor blades respectively.}$$

$$D = \sqrt{\frac{A \times 4}{\pi}} = \sqrt{\frac{1423.0577 \times 4}{\pi}} = \mathbf{42.5663m}$$

The Radius of the wind turbine blades is obtained as $\frac{Diameter}{2} = \frac{42.57}{2} = 21.2832m$

Considering a rotor radius of 21.285m, it allows for a clearance of 18.715m, and hence, only One wind turbine is required to supply power to the factory, and it is a grid-integrated wind turbine.

- *Estimation of Rotational Speed of the Designed Wind Turbine*

One important parameter to be considered when designing a wind turbine is the tip speed ratio. The tip speed ratio refers to the ratio between the wind speed and the speed of the tips of the wind turbine blades. Mathematically, the tip speed ratio is expressed as,

$$TSR(\lambda) = \frac{\text{Rotational Speed of the blade} \times \text{Radius of blade}}{\text{Wind Speed}} = \frac{\omega r}{v} \tag{15}$$

For a wind turbine that has three blades made with carbon fiber, the tip speed ratio is usually between 6 – 7 [9]. Hence, assuming a tip speed ratio of the designed wind turbine is 7, the rotational speed, ω can be derived from equation 16 above as,

$$\omega = \frac{\lambda V}{r} = \frac{7 \times 7.05}{21.2832} = 2.3187m/s \sim \mathbf{22.1420rpm}$$

ISSN No:-2456-2165 https://doi.org/10.38124/ijisrt/26aug308

➢ *Estimation of Gear Box Ratio Requirement of the Wind Turbine*

The generator to be designed for this wind turbine has a rated speed of 1500 rpm. The gear The ratio of the gearbox is estimated as follows.

$$\text{Gearbox ratio (N)} = \frac{\text{Speed of the Generator Shaft}}{\text{Speed of the Wind Turbine's Shaft}} = \frac{\omega_S}{\omega_T} \qquad (16)$$

Where, $\omega_s = 1500$rpm and $\omega_T = 22.1420$ rpm

$N = \frac{1500}{22.1420} = 67.74 \sim \mathbf{68}$ Hence, the gearbox ratio of the low-speed shaft of the wind turbine to the high-speed shaft of the generator is 1:68.

➢ *Consolidated Specification of the Designed Wind Turbine*

The table below provides a summary of the various parameters of the designed wind turbine.

Table 5 Consolidated Specification of the Designed Wind Turbine.

Component	Parameter	Specification
Power	Rated Power	115.04kW
	Cut-in Wind - Speed	1.5m/s
	Rated Wind Speed	7.05m/s
	Cut-out- Wind Speed	28m/s
	Wind Class (IEC)	III
Rotor	Diameter	42.571m
	Swept Area	1423.06m^2
	Number of Blades	3
	Rotor Speed	22.14rpm
	Tip Speed	49.35m/s
Gear Box	Type	Geared Box Wind Turbine
	Ratio	1:68
Generator	Type	Radial Flux PM Alternator
	Number	1
	Speed	1500rpm
	Voltage	433V
	Grid frequency	50Hz
	Grid Connection	Grid Connected
Tower	Hub Height	40m
	Shape	Tubular Steel
	Corrosion Protection	Painted

➢ *Performance Characteristics Curves of the Designed Wind Turbine.*

The designed wind turbine is a variable-speed wind turbine. A variable-speed wind turbine is specifically designed to operate over a wide range of rotor speeds. This design ensures that the wind turbine generates maximum aerodynamic power from the wind at varying wind speeds. It is common knowledge that the electrical power generated by the wind turbine is dependent on the wind speed and that as the wind speed increases or decreases, the output power is affected. Notwithstanding, due to the variability of the wind, harnessing more wind energy does not only involve enhancing the mechanical properties of the wind turbine, but also improving the control methods used. To understand MMPT control algorithms, let's consider a wind turbine system overview below.

ISSN No:-2456-2165 https://doi.org/10.38124/ijisrt/26aug308

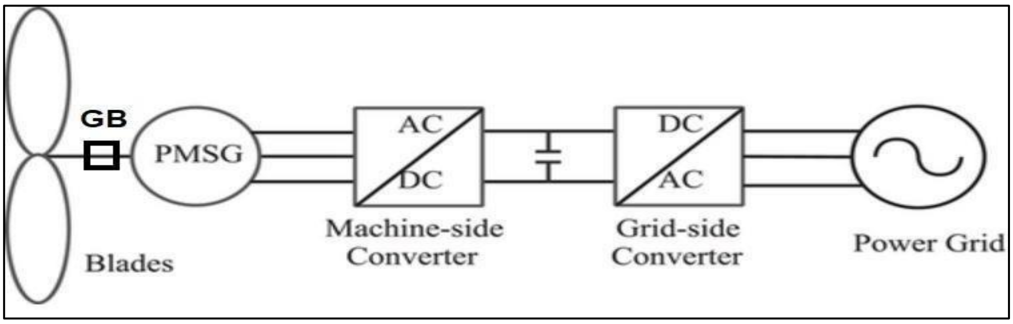

Fig 5 Overview of a Wind Turbine System[16].

The wind blades convert the kinetic energy in the wind into mechanical energy, which is subsequently converted into electrical energy by the generator. Mechanical power captured by the wind turbine is given as Pmech = $\frac{1}{2}\rho A v^3 C_p(\lambda, \beta)$. The power coefficient cp is a function of the blade tip speed ratio λ and pitch angle β. The tip speed ratio, which is given as $\lambda = \frac{\omega_t R}{v}$, can be written in terms of wind speed, v as $\frac{\omega_t R}{\lambda}$. Therefore, the mechanical power, Pmech = $\frac{1}{2}\rho A \frac{\omega_t^3 R^3}{\lambda^3} C_p(\lambda,\beta)$. Generally, cp is considered as a non-linear function of tip speed ratio and pitch ratio and pitch angle of the blades, which is given as $C_p(\lambda,\beta) = (0.44 - 0.016\beta)\sin\left(\frac{\pi(\lambda-3)}{15-0.3\beta}\right) - 0.00184(\lambda-3)\beta$.[13] When the wind speed is lower than the rated wind speed i.e., β = 0,° the power coefficient curve is then shown as.

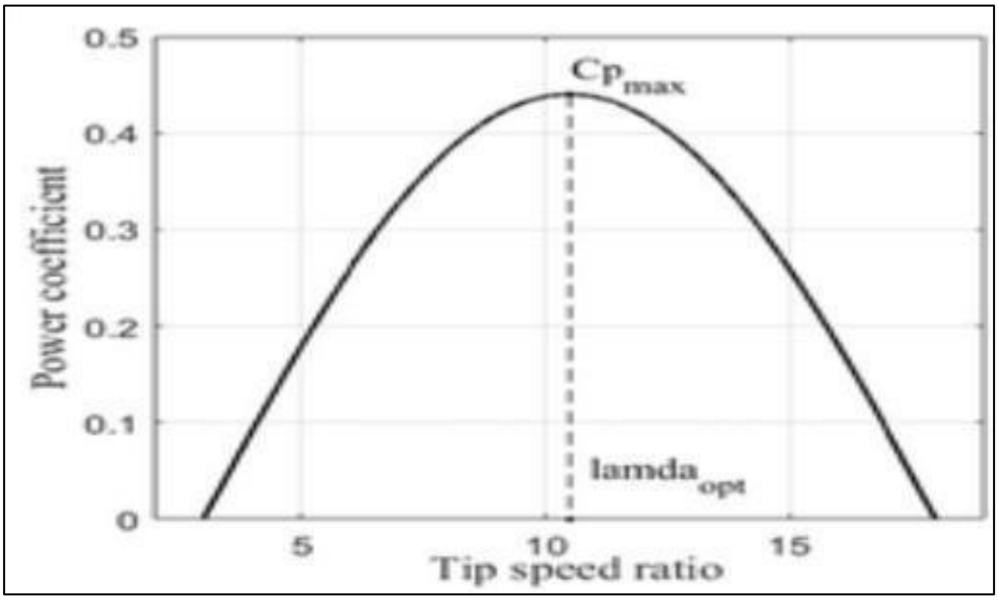

Fig 6 Power Coefficient Curve of a Wind Turbine [16].

The MMPT control algorithm is used to adjust the generator's rotor speed in response to variations in wind speed, keeping the wind turbine operating at the ideal tip speed ratio(λopt), that is to say that Cp is always maintained at or close to Cpmax to obtain more power and capture more wind energy. The majority of these widely utilized algorithms nowadays can be divided into four categories, namely, tip speed ratio (TSR) algorithm, hill climbing search (HCS)/perturb and observe (P&O) algorithm, optimal torque (OT)/power signal feedback (PSF) algorithm, and hybrid and intelligent (H&I) algorithm [13].

ISSN No:-2456-2165 https://doi.org/10.38124/ijisrt/26aug308

CHAPTER FIVE
DESIGN OF THE WIND TURBINE GENERATOR

➢ *Analytical Design of a Generator for the Proposed Wind Turbine*

This will involve the use of mathematical equations and assumptions in defining the various geometric parameters of the proposed generator. But before designing, some basic decisions and parameters are made. These parameters and decisions influence the generator to be designed. The discussions below explain some of the designed decisions and parameters.

➢ *Type of Excitation of the Generator*

In producing a rotating magnetic field, the synchronous generator should have an excitation system. There are mainly two ways of producing the excitation: supplying direct current to a wound rotating field through slip rings and brushes, or using a permanent magnet. In this design, permanent magnets are used to provide the rotating magnetic field.

➢ *Permanent Magnet Configuration*

Synchronous machines with permanent magnet rotors are increasingly used in high-speed applications [14]. Based on how the permanent magnets are placed on the rotor, the machine can broadly be categorized as having Interior Permanent Magnet (IPM) or Surface Mounted Permanent Magnet (SPM) [14] IPMs are embedded within the iron core of the rotor, whereas in SPM's the permanent magnets are attached to the outer surface of the iron core. SPM rotors allow higher rotational speeds than IPM rotors. [14]. Since a gearbox is used to increase the speed of the rotor, a surface-mounted permanent magnet is used for this design.

➢ *Selection of Permanent Magnets*

Permanent magnets are magnets that can retain magnetic properties in the absence of an inducing field or current. Permanent magnets should have high remanence Br, or magnetization remaining after the applied magnetic field is removed. It should also have high coercivity (Hc) or resistance to demagnetization. In most commercial applications of permanent magnets, an important factor is given to the magnets with high energy production or energy density.[15]. For instance, in wind turbine applications, generators made up of permanent magnets should have high power density. In selecting the type of permanent magnet to be used in this generator design, a comparison was made among the properties of magnets made up of rare-earth and non- rare earth metals. The four most commercially used permanent magnets, namely, Neodymium Iron Boron (NdFeB), Samarium Iron Cobalt (SmCo), Hard Ferrites, and Alnico magnets, were selected, and their properties compared in the table below. The highest grades of these permanent magnets with a data sheet obtained from www.eclipsemagnetics.co, were compared.

Table 6 A Table Comparing Four Commercially Used Magnetic and their Properties.

Magnet	**Grade**	**Br (Kg)**	**Hc (Koe)**	**BHmax (MGOe)**	**Tm (℃)**
NdFeB	N52	14.3	10.00	50	220
SmCo	SmCo30H	11.0	10.5	30	350
Hard Ferrites	Y40	4.6	4.45	5.3	300
Alnico	Alnico9- LNDT80	10.8	1.5	10	550

NdFeB permanent magnets are considered far superior to other permanent magnets for PM generators as they have the highest available energy product. [15]. NdFeB corrodes easily therefore requiring a coating in most applications including wind turbines. On the other hand, SmCo magnets do not corrode as easily, but are more expensive and have lower maximum energy products as compared to NdFeB [15]. Hard ferrites and alnico are non-rare earth and are therefore less expensive as compared to NdFeB and SmCo but have lower energy products and require significantly more volume to achieve the equal magnetic flux density as NdFeB or SmCo. Conclusively, since the permanent magnet required for the wind turbine generator must have a high energy density, NdFeB is selected for the design.

➢ *Selection of Materials for the Construction of a Generator*

In this aspect, magnetic materials are considered for the construction of the stator and the rotor. About the stator-rotor configuration of the proposed machine, the armature winding will be on the stator, whereas the field will be on the rotor. Because of that, the magnetic material to be used for the rotor back iron must have a low magnetic loss to retain enough magnetic flux to improve the efficiency of the machine. On the other hand, the stator core must have a high saturation point to receive as much magnet flux as will be produced by the permanent magnets on the rotor. The selection of a suitable material is carried out by comparing the BH curves of the various magnetic materials available in the ANSYS MOTOR CAD software. Amon 7.3. 25% Si was found to have the highest magnetic flux density at a very high magnetic field intensity. The BH curve of Amon 7.3.25% Si is presented below.

ISSN No:-2456-2165 https://doi.org/10.38124/ijisrt/26aug308

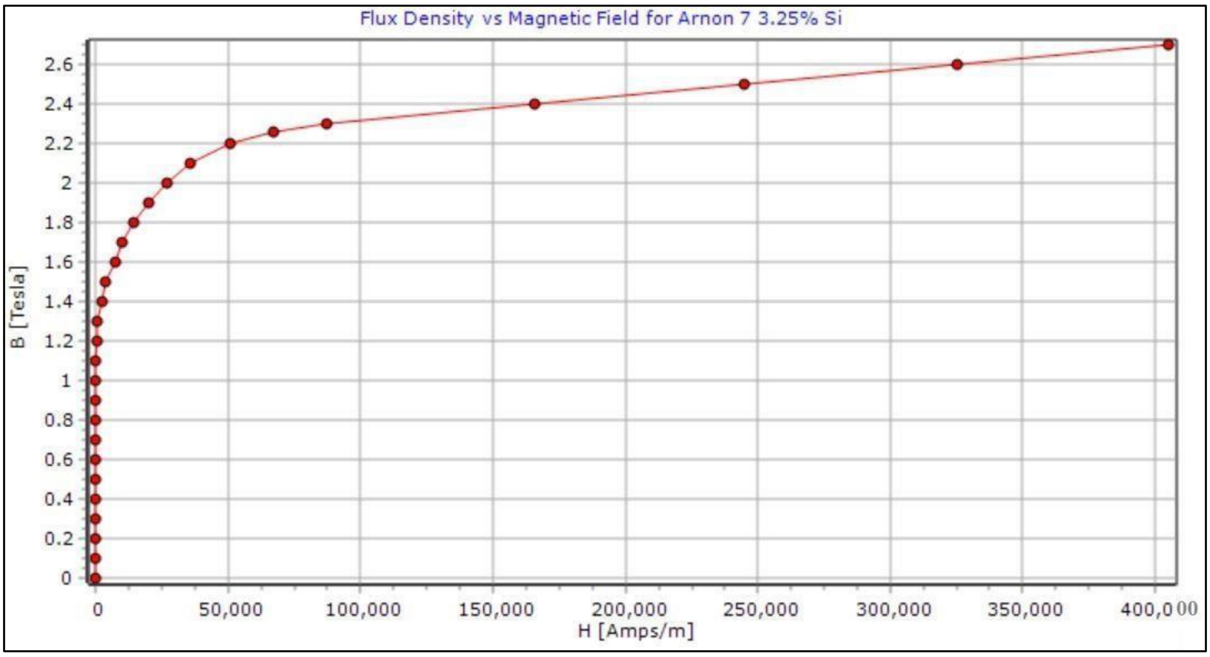

Fig 7 BH Curve of Amon 7.3. 25% Si.

The material required for the winding configuration of the stator should have low resistivity but high conductivity. Hence, the material chosen for the stator's winding is copper and it has the specifications as shown in table 5.2 below.

Table 7 A Table of Copper Winding and its Specifications.

Parameter	**Value**
Resistivity @ 20˚C (ohm.m)	1.724E-8
Thermal Conductivity (W/m/˚C)	401
Specific Heat (J/kg/˚C)	385
Density (kg/m^3)	8933

➢ *Types of Rotor Placement*

Depending on how the rotor is placed inside the machine, the types of rotors can be classified into outer rotor and inner rotor. In the outer rotor machines, the rotor is on the outside and the stator is on the inside of the machine. Comparatively, in the inner rotor machines, the rotor is in the interior of the machine and the stator is on the outside of the machine. Both arrangements have their advantages and disadvantages. The rotor placement will affect the temperature rise of the machine. Since the cooling system is often placed outside of the machine, the stator of the machine will undergo much heating due to current flow in the stator windings and eddy current losses. Since the power rating is low and air cooling will be employed, an inner rotor type is selected for this design.

➢ *Determination of the Number of Poles and Stator Slots*

Many factors contribute to the choice of the number of poles required for a generator of a brushless generator. The magnetic material and grade, interior rotor versus exterior rotor versus axial-gap rotor, mechanical assembly of the rotor, speed of rotation, and inertia requirements all contribute to the choice of pole selection.[16] In this case, since the synchronous speed of the rotor is already known to be 1500rpm, the number of poles of the generator is estimated as follows.

$$N_{sync} = \frac{120f}{P} \tag{17}$$

$P = \frac{120f}{N_{sync}}$, Where Nsync. = Synchronous speed = 1500rpm f = frequency = 50Hz.

$$P = \frac{120 \times 50}{1500} = 4\ \boldsymbol{poles}$$

The selection of stator slots for a brushless generator considers a possible alignment for slots and poles that will resist cogging

ISSN No:-2456-2165 https://doi.org/10.38124/ijisrt/26aug308

[16]. Another consideration is the winding pitch. Considering these two factors, **24** slots are selected. Hence, the number of slots per pole per phase is 2.

➢ *Estimation of Rotor Diameter at Airgap and Stack Length*

In this section, the calculation of the machine's rotor diameter at the airgap and its stack length is estimated. From equations 12 & 13 above, the input mechanical power of the lowspeed shaft of the wind turbine is 107.3108A W/m^2. Due to the use of a gearbox which is assumed to be 93% efficient, the input mechanical power of the high-speed shaft to the generator then becomes 99.7990W/m^2 i.e. (107.3108A W/m^2 ×0.93 = 99.7990A W/m^2). The swept area of the designed wind turbine has been determined in Equation 13 above as 1423.0577m^2.

Pmech = 99.7990**A** = 99.7990W/m^2 × 1423.0577m^2 = 142.0197kW

Mechanical Power to the Generator (Pmech) = Torque (T) × Rotational speed of the rotor (ω)

$$Pmech = T\times\omega \tag{18}$$

$$T = \frac{Pmech}{\omega}, \qquad \text{but } \omega = 1500\text{rpm which equivalent to } 1500 \times \frac{2\pi}{60}\ \text{rads/s}$$

$$\frac{142.0197 \times 10^3}{1500 \times \frac{2\pi}{60}} = \mathbf{904.1255N.m}$$

The torque equation of a machine is given as,

$$T = \frac{\pi}{2} D^2 L B_{rms} A k_w \ldots \tag{19}$$

Where, T = Input Torque

A = Electric loading

D = Diameter of the rotor at the airgap

B = rms magnetic loading

L = Stack length of the machine

k_w = Winding factor

$$k_w = \frac{\sin\left(\frac{\pi}{6}\right)}{q\sin\left(\frac{\pi}{6q}\right)} \tag{20}$$

Where q = number of slots per pole per phase = $\frac{z}{2\times m\times p}$, m = number of phases = 3

p = number of pole pairs = 2 and z = number of slots = 24.

q = 2, each $\frac{24}{2\times3\times2}$ pole will have two slots dedicated for each phase.

$$k_w = \frac{\sin\left(\frac{\pi}{6}\right)}{2\times\sin\left(\frac{\pi}{6\times2}\right)} = \mathbf{0.9659}$$

From equation 20 above, the diameter of the rotor at the airgap depends on the magnetic loading(B) and electric loading(A). These are empirically defined at the preliminary stage of the machine design. However, in choosing parameters for these two, consideration is given to iron losses. Choosing a high value for B will lead to high magnetic flux density in the stator teeth and core.

ISSN No:-2456-2165 https://doi.org/10.38124/ijisrt/26aug308

This increases hysteresis losses and eddy current losses leading to high iron losses and temperature rise which will subsequently decrease the efficiency of the machine. On the other hand, for a value of A, copper losses and temperature rise in the armature winding were the primary considerations. Electric loading depends on the current flowing through the windings and the number of turns of the windings which means an increase in A is either by increasing the current flowing through the windings or by increasing the number of turns. Either of these two will lead to high I^2R losses which will equally lead to a rise in the temperature of the machine thereby reducing the efficiency of the machine. By considering these factors, moderate values are chosen for these parameters. For non-salient pole synchronous machines, air-gap magnetic flux density ranges between 0.8 – 1.05T whereas electric loading for air cooling machines ranges between 30 – 80kA/m [17]. Hence, 0.9T and 30kA/m are chosen for B and A respectively. Finally, another important parameter considered is the aspect ratio of the proposed machine. Though in cylindrical machines, D and L are essentially independent variables the ratio of the stack length to diameter is usually between 1- 1.5 [17]. Hence, the L/D ratio is taken as 1.5. From Equation 20 above, the torque equation can be written as,

$$D^2 = \frac{2T}{\pi L B_{rms} A k_w}$$

$B_{rms} = \frac{B_{peak}}{\sqrt{2}} = \frac{0.9}{\sqrt{2}} = 0.6364T$ and L/D = 1.5, T = 904.1255N.m A = 30kA/m $k_w = 0.9659$

$$D^2 = \frac{2 \times 904.1255}{\pi \times 1.5 \times D \times 0.6364 \times 30 \times 10^3 \times 0.9659}$$

$$D^3 = \frac{2 \times 904.1255}{\pi \times 1.5 \times 0.6364 \times 30 \times 10^3 \times 0.9659}$$

$$D = \sqrt[3]{\frac{2 \times 904.1255}{\pi \times 1.5 \times 0.6364 \times 30 \times 10^3 \times 0.9659}}$$

D = 0.2750m

The stack length of the proposed machine can be determined as,

L = 1.5 × D

= 1.5 × 0.2750m

= 0.4126m.

Hence, the proposed machine’s rotor diameter at the airgap and stack length is 0.2750m and 0.4126m respectively.

- *Estimation of Magnetic Thickness*

By employing the use of four poles NdFeB magnets. The thickness of these magnets to produce the required magnetic flux is estimated below. The analysis is carried out using the diagram below.

ISSN No:-2456-2165 https://doi.org/10.38124/ijisrt/26aug308

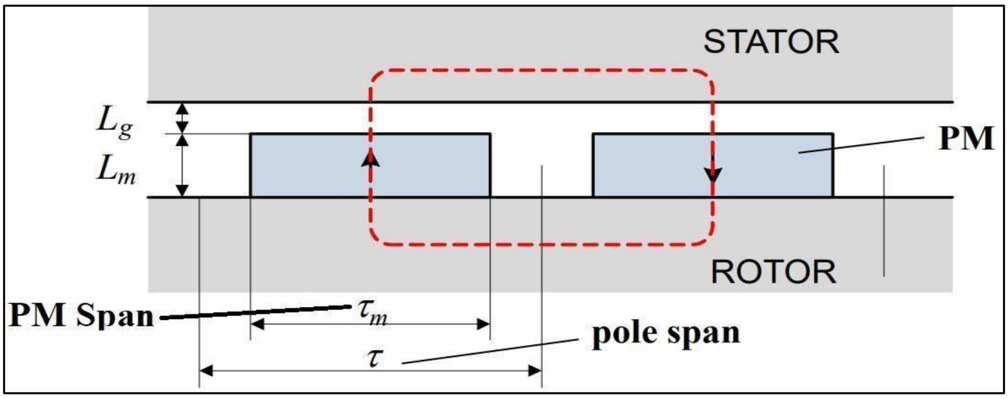

Fig 8 Cross Sectional View of the Generator's Interior View for the Estimation of Magnet.

$$B_m = B_r + \mu_m \mu_o H_m. \quad (21)$$

$$H_m L_m + H_g L_g = 0$$

$$B_m = B_g$$

The magnetic flux density at the airgap is obtained as,

$$B_g = \frac{B_r}{1 + \mu_m \frac{L_g}{L_m}} \quad (22)$$

B_g = Magnetic flux density at the airgap

L_g = Airgap length

B_r = Magnet remanent flux density

L_m = Magnet thickness

μ_m = Permeability of the magnet

Considering how the permanent magnets are mounted on the rotor as demonstrated in the figure below, if the magnetic span, α is less than the pole span, τ then the flux density at the airgap is related to the peak flux density as,

$$B_{peak} = B_{max} = \frac{4}{\pi} B_g \sin\left(\frac{\alpha}{2}\right) \quad (23)$$

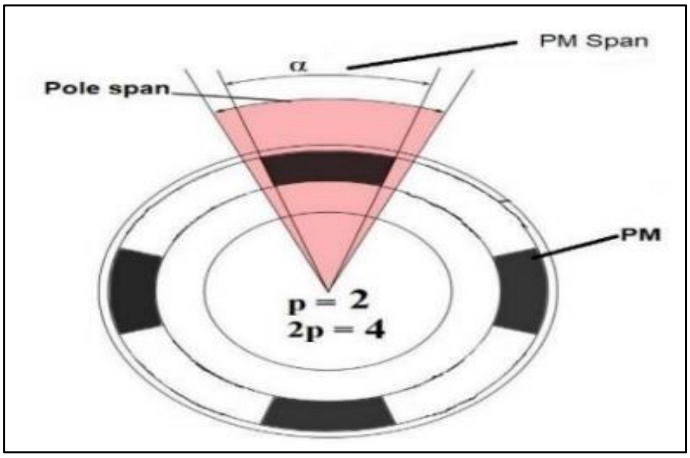

Fig 9 Magnet Arrangement on Rotor.

ISSN No:-2456-2165 https://doi.org/10.38124/ijisrt/26aug308

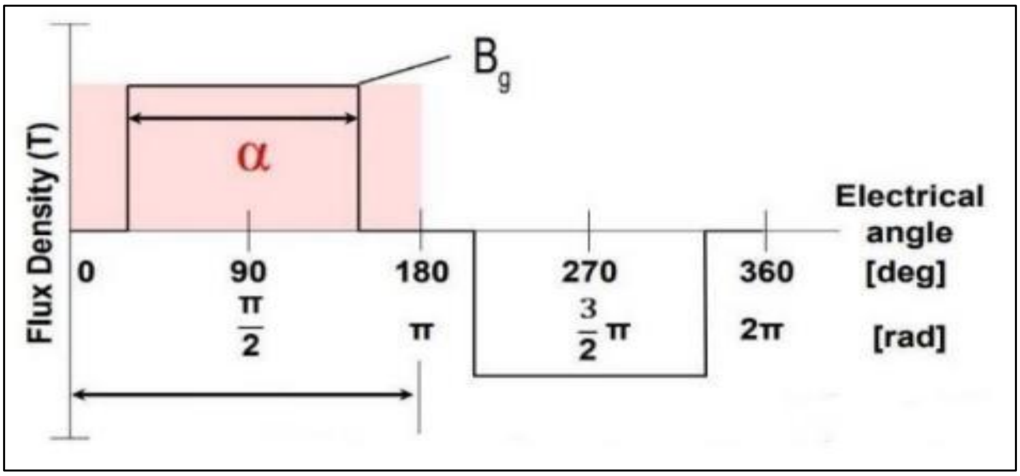

Fig 10 Flux Density Against Electrical Angle [Degree].

From Figure 10 above, it is clear that the magnet span is less than the pole span. Hence, the ratio of magnet span to pole span is given as;

$$k_a = \frac{\tau_m}{\tau} \tag{24}$$

Referring to Figure 6 and Equation 25 above, the ratio of the magnet span to the pole span can be written as;

$$k_a = \frac{\tau_m}{\tau} = \frac{\alpha}{\pi} \qquad \alpha = \pi k_a \tag{25}$$

Substituting Equation 26 into Equation 24;

$$B_{peak} = \mathrm{Bmax} = \frac{4}{\pi} B_g \sin\left(\frac{\pi k_a}{2}\right)$$

B_{max} = 0.9T and taking 0.8 as the ratio of magnet span to pole span.

$$0.9 = \frac{4}{\pi} B_g \sin\left(\frac{\pi \times 0.8}{2}\right)$$

$$\mathrm{Bg} = \frac{0.9}{1.2109} = \mathbf{0.7432T}$$

As discussed above, NdFeB is selected for the design of the generator. In the ANSYSMOTOR CAD Software, N48H_AM is selected for the design. It has the following properties. The airgap length (L_g) is taken as 1mm.

.

Table 8 A Table of N48H_AM Properties as Stated in the ANSYS-MOTOR CAD Software.

Magnet Parameter	Specification
Magnet Remanent Flux Density B_r	1.39T
Magnet Relative Permeability(μ_m)	1.04
Electrical Resistivity	1.4×10^{-6} $0hm$.m

Recalling from equation 23 above; $B_g = \dfrac{B_r}{1 + \mu_m \frac{L_g}{L_m}}$

ISSN No:-2456-2165 https://doi.org/10.38124/ijisrt/26aug308

$$B_g + B_g \mu_m \frac{L_g}{L_m} = B_r \,; \qquad \frac{L_g}{L_m} = \frac{B_r - B_g}{B_g \mu_m} \,; \qquad L_g\,(B_g \mu_m) = L_m (B_r - B_g)$$

$$L_m = \frac{L_g\,(B_g \mu_m)}{(B_r - B_g)} \qquad L_m = \frac{1 \times 10^{-3}\,(0.7432 \times 1.04)}{1.39 - 0.7432} = \mathbf{1.1950 \times 10^{-3} m}$$

To avoid demagnetization and any field deterioration the magnet thickness is increased by a factor of 3. Hence, the magnet thickness required is taken as $\mathbf{3.585 \times 10^{-3} m}$.

➤ *Calculation of Rotor Back Iron and Shaft Diameter*

As discussed above, the material selected for the construction of the rotor back iron, stator teeth, and yoke is Amon 7.3. 25% Si. For non-salient pole synchronous machines, the rotor yoke flux density is between 1.3 to 1.6T.**[**17**]**. The rotor yoke flux density ($B\lambda$) is chosen as

1.6T. The thickness of the rotor back iron is given as;

$$R_{back} = \frac{B_{av} \times \tau_P}{2 \times B_\lambda} \tag{26}$$

$$\tau_p = \frac{\pi D}{2p} \tag{27}$$

Bav = Average Magnetic loading = 0.6364T

D = Diameter of rotor at airgap = 0.2750m

τ_p = Pole span

B_λ = Rotor back iron flux density = 1.6T

$$\tau_p = \frac{\pi \times 0.2750}{2 \times 2} = \mathbf{0.2160 m}$$

$$R_{back} = \frac{0.6364 \times 0.2160}{2 \times 1.6} = \mathbf{0.0430 m}$$

Diameter of Shaft = Diameter of Rotor at the Airgap - $2 \times R_{back}$ - $2 \times L_m$

= 0.2750 – (2×0.0430) – (2 × 3.585 ×10^{-3})

= **0.1818m**

The rotor back iron and shaft diameter should have a thickness of 0.0430m and 0.1818mm.

➤ *Determination of Stator Tooth and Width*

With an already determined material for the construction of the stator, the stator back iron and tooth width. Their various dimensions are estimated using the diagram below for analysis.

ISSN No:-2456-2165 https://doi.org/10.38124/ijisrt/26aug308

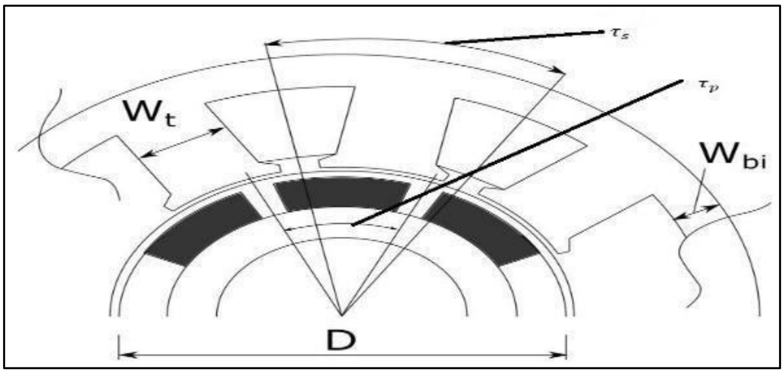

Fig 11 Cross-Sectional Area of a Generator Showing Poles and Stator Tooth and Slots.

Figure 11 above, Wt = Stator tooth width

D = Diameter of the rotor at airgap

τs = Slot pitch

τp = Pole pitch

W_{bi} = Stator back iron width

$$\tau_s = \frac{\pi \times D}{Z} \tag{28}$$

Where Z = Number of stator slots = 24

$$\tau_s = \frac{\pi \times 0.2750}{24} = \mathbf{0.0360m}$$

The tooth width is calculated using the relation $W_t = \frac{B_{av} \times \tau_s}{B_t}$, where B_t = Magnetic flux density at stator teeth. For non-salient pole synchronous machines, the average maximum flux density is between 1.5 – 2.0T [17]. Hence, the tooth flux density is taken as 1.6T. Additionally, the stator yoke flux density ranges between 1.1 – 1.5T [17]. It is assumed that the flux in the stator back iron is less than the stator teeth since the flux coming from the permanent magnets divides in the stator back iron. Hence, the flux density (B_{bi}) in the stator back iron is taken as 1.4T.

$$W_t = \frac{0.6364 \times 0.0360}{1.6} = \mathbf{0.0143}$$

Hence, the stator tooth width is 0.0143m.

The width of the stator back iron is calculated as;

$$W_{bi} = \frac{1}{2} \cdot \frac{B_{av} \times \tau_p}{B_{bi}}, \text{ where } B_{bi} = 1.4T$$

$$W_{bi} = \frac{1}{2} \cdot \frac{0.6364 \times 0.2160}{1.4}$$

= 0.0491m

Hence, the width of the stator back iron is obtained as 0.0491m.

ISSN No:-2456-2165 https://doi.org/10.38124/ijisrt/26aug308

➢ *Calculation of Slot Area and Slot Inner Diameter*

To estimate the slot area and slot inner diameter, the diagram below is employed to perform the analysis.

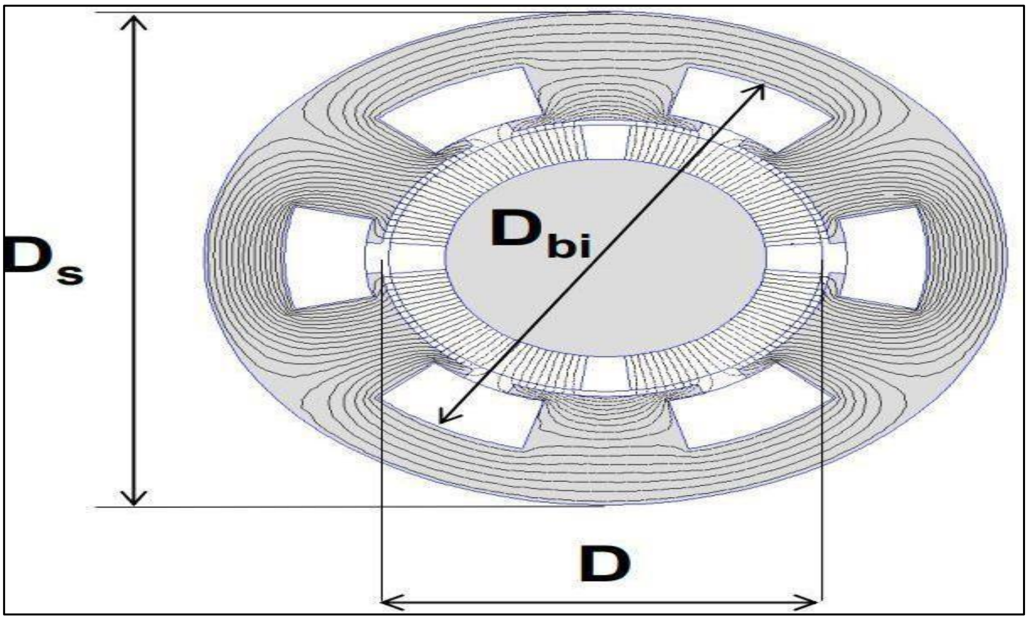

Fig 12 Cross Sectional View of a Four-Pole Generator Showing Various Diameters.

From Figure 12 above, D_{bi} = Slot inner diameter, D_s = Outer diameter.

It is taken that the inner area of the stator iron is equally shared between the stator teeth and slots, which are occupied by the copper windings. Hence, the area occupied by all slots is calculated as.

$$S_{all\_slots} = \frac{1}{2} \cdot \frac{\pi}{4} (D_{bi}^2 - D^2) \tag{29}$$

$$\text{Dbi} = \sqrt[2]{\frac{8 S_{all\_slot}}{\pi} + D^2}$$

$$D_S = D_{bi} + 2W_{bi} \tag{30}$$

Also, the electric loading (A) is given as.

$$\text{A} = \frac{J . S_{all\_slots} . k_{fill}}{\pi D} \tag{31}$$

$$\text{A} = \frac{2. m. N_{ph}. I}{\pi D} \tag{32}$$

A = Electric loading = $30{\times}10^3$A/m J = Current density I = Current

N_{ph} = Number of turns per phase $kfill$ = slots fill factor (area of copper/area of slot) = 0.45 For a non-salient pole synchronous machine with air cooling, the current density (J) is between 3 – 5A/mm^2 [17]. Therefore, the chosen current density J is 3A/mm^2

ISSN No:-2456-2165 https://doi.org/10.38124/ijisrt/26aug308

($3\times10^6 A/m^2$).

Recalling from equation 32; $A = \frac{J.S_{all\ slots}.k_{fill}}{\pi D}$

$$S_{all\_slots} = \frac{A\pi D}{J.k_{fill}}$$

$$S_{all\_slots} = \frac{30\times10^3 \times \pi \times 0.2750}{3\times10^6 \times 0.45}$$

$= 0.0192m^2$

Recalling from equation 30; $Dbi = \sqrt[2]{\frac{8\,S_{all\_slot}}{\pi} + D^2}$

$$Dbi = \sqrt[2]{\frac{8(0.0192)}{\pi} + (0.2750)^2}$$

$= 0.3529m$

The slot depth, $D_{slot\ depth} = \frac{Dbi - D}{2}; \frac{0.3529 - 0.2750}{2}$

$= \mathbf{0.03895m}$

Stator outer diameter is given as; $D_s = D_{bi} + 2W_{bi}$

$D_s = 0.3529m + 2(0.0491)m$

= 0.4511m

➢ *Power and Number of Turns Calculations*

The peak power required by the factory is 115.036kW. The factory is supplied with power at a voltage of 433V phase voltage. Hence, the generator's terminal voltage required is taken as 433V as it is delta-connected. The generator is made with a permanent magnet, which ideally has a unity power factor, but in the worst case, the generator's power factor is taken as 0.9.

Hence, the kVA rating of the generator is estimated as,

$P = 3I_P V_P \cos\theta$; I_p = Phase current, V_p = Phase voltage, $\cos\theta$ = Power factor = 0.9,

$S = 3I_pV_p$ $P = S\cos\theta$ P = Real power (kW) = 115.036kW S = Apparent power (kVA)

$$S = \frac{P}{\cos\theta} = \frac{115.036\times10^3}{0.9} = \mathbf{127.8178kVA}$$

$$I_p = \frac{s}{3\times V_P} = \frac{127.8178\times10^3}{3\times433} = \mathbf{98.3971A}$$

As discussed above, copper is used for the winding in the stator slots. It has a resistivity of 1.724E-8 Ohm.m. The length of the end windings (*Lew*) depends on the winding configuration and connection. In this analysis, the end winding is taken as a concentrated winding. The resistance per phase of the copper is determined as follows,

ISSN No:-2456-2165 https://doi.org/10.38124/ijisrt/26aug308

Where: $L* = L + L_{ew}$; $L_{ew} = 2.5(\frac{D}{2})$ where, L^* = motor length and L = Active Length

$$L^* = 0.4126 + 2.5\left(\frac{0.2750}{2}\right) = \mathbf{0.7564m}$$

ρ_{cu} = Copper resistivity = 1.724E-8 Ohm.m S_{all_slots} = Area of all slots filled = 0.0192m^2

$$P_{copper\_loses} = \rho_{cu} \times L^* \times S_{all\_slots} \times k_{fill} \times J^2$$

$$= 1.724 \times 10^{-8} \times 0.7564 \times 0.0192 \times 0.45 \times (3 \times 10^6)^2$$

$$= \mathbf{1013.9495W}$$

$$P_{copper\_loses} = 3.I_P^2.R; \qquad R = \frac{P_{copper\_losses}}{3.I_P^2}$$

$$R = \frac{1013.9495}{3 \times (98.3971)^2} = \mathbf{0.0350\ Ohms}$$

The voltage induced in the stator windings depends on the magnetic flux density in the airgap, speed of rotation of the rotor, and number of turns of the windings. The peak induced voltage is expressed as,

$$E_A = 2\pi f N_{Ph} B_{max} k_w \frac{DL_{stack}}{p} \tag{33}$$

Where N_{ph} is the number of turns per phase.

Equating equations 31 and 32; $\frac{J.S_{all\_slots}.k_{fill}}{\pi D} = \frac{2.m.N_{ph}.I}{\pi D}$;

$2.m.Nph.IP = J.Sall\_slots.kfill$

$$N_{Ph} = \frac{J.S_{all\_slots}.k_{fill}}{2.m.I_P}$$

$$N_{ph} = \frac{3 \times 10^6 \times 0.0192 \times 0.45}{2 \times 3 \times 98.3971}$$

Nph = 43.9037 approximately 44 turns.

Turns per slot (N); $\frac{\text{Number of turns per phase}}{\text{Number pole pair} \times \text{slot per pole per phase}} = \frac{44}{2 \times 2} = \mathbf{11\ turns}$

From Equation 33 above, the peak-induced voltage can be calculated as,

$$E_A = 2\pi \times 50 \times 44 \times 0.9 \times 0.9659 \times \frac{0.2750 \times 0.4126}{2}$$

= 681.7249V

Hence, the peak-induced voltage is 681.7249V and its RMS value is obtained as,

ISSN No:-2456-2165 https://doi.org/10.38124/ijisrt/26aug308

$$E_{RMS} = \frac{E_{peak}}{\sqrt{2}} = \frac{681.7249}{\sqrt{2}} = 482.0523V$$

➢ *Temperature Rise of the Designed Generator*

The designed generator will use air as its cooling method through the process of convection. The main sources of heat will be I^2R loss in the copper windings and the iron losses. The copper losses were calculated above as 1013.9495W. It is taken that the copper loss is the same as the iron loss. The temperature is calculated as,

Exterior Area = $\pi D_{ext} L^*$, where D_{ext} = External diameter = 0.5149m L^*= Total length of the machine including end windings = **0. 7564m**.

Exterior Area = π × 0.5149 × 0.7564 = 1.2236m^2

$$\text{Heat Convection Transfer Coefficient} = h = \frac{2 \times \textit{Copper Loss}}{70 \times \textit{Exterior Area}} = \frac{2 \times 1013.94}{70 \times 1.2236}$$

$$= 23.6758 W/℃.m^2$$

$$\text{Temperature Rise} = \frac{2 \times \textit{Copper Loss}}{h \times \textit{Exterior Area}} = \frac{2 \times 1013.94W}{23.6758W/℃.m2 \times 1.2236m^2} = 70^{\circ}C$$

➢ *Calculating the Efficiency of the Designed Machine*

The efficiency of a machine determines the performance of the machine. It is the ratio of the output of the machine to the input of the machine**.** Mathematically, efficiency is expressed as,

$$\text{Efficiency} = \frac{\textit{Output Power}}{\textit{Input Power}} \times 100\%$$

The Input Power to the Generator = Torque × Mechanical Rotation = T × ω

$$\text{Torque} = 904.1255\text{N.m} \qquad \omega = 1500\text{rpm} \left(1500 \times \frac{2\pi}{60} \right)$$

$$P_{input} = 904.1255 \times 1500 \times \frac{2\pi}{60} = 142.01947kW$$

The Losses of the Machine = Copper Losses + Mechanical losses + Core Losses

The core losses are taken to be the same as the copper losses and the mechanical losses are ignored. Hence, the total input power can be expressed as,

Total Input Power = Output Power + 2 × Copper Losses

Output Power = Total Input Power – 2 × Copper Losses

$$\text{Efficiency} = \frac{\text{Total Input Power} - 2 \times \text{Copper Losses}}{\textit{Input Power}} = \frac{142.0194 \times 10^3 - 2(1013.94)}{142.0194 \times 10^3}$$

= **0. 9857 ~ 98. 57**

Conclusively, Chapter 5 above presents the analytical calculations of the proposed generator. In addition, a MATLAB script has been developed to perform all calculations should a parameter be changed. In the case where the wind turbine generates less than the factory's peak load, energy will be drawn from the grid to support the load demand of the factory. Alternatively, if the wind turbine operates at rated conditions where power exceeds load demands, the excess power will be fed into the grid. A wind turbine power converter that produces constant voltage and frequency from varying wind speeds is a back-to-back ACDC-AC power electronic converter, often implemented using Pulse Width Modulation (PWM). These will later be considered in detail in another piece of research work.

ISSN No:-2456-2165 https://doi.org/10.38124/ijisrt/26aug308

CHAPTER SIX
VALIDATION OF THE DESIGNED WIND TURBINE GENERATOR

➢ *Design Analysis Using Computed Aided Design Software*

Following the completion of the analytical calculations for the proposed generator, ANSYS MOTOR CAD version 12.1.1 software is employed to perform the Finite Element Analysis of the proposed generator. The use of this software requires the entry of parameters obtained from the analytical calculations. Under the electromagnetic model tab, the following tabs are filled out based on the calculated parameters. The geometry tab, winding tab, Input data tab, and calculation tab. The section below presents the various parts and their values.

➢ *The Geometry Input Tab*

This is used to define the machine geometry in the axial and radial views. Based on the parameters calculated in the analytical design, the table below provides the values of the various dimensions of the generator.

Table 9 Radial Geometry for Stator and Rotor Parameters In the ANSYS MOTORCAD Software.

Stator Parameter	**Value**	**Rotor Parameters**	**Values**
Slot type	Parallel tooth	Rotor type	Surface Radial
Stator Ducts	None	Rotor Ducts	None
Slot number	24	Pole Number	4
Stator Lam. Diameter	451.1mm	Magnet thickness	3.585 mm
Stator Bore	276 mm	Magnet Reduction	0 mm
Tooth Width	14.30 mm	Magnet Arc	165˚
Slot Depth	38.95 mm	Magnet Segment	1
Slot Corner Radius	2 mm	Airgap	1 mm
Tooth Tip Depth	2 mm	Banding Thickness	0
Slot opening	3 mm	Shaft Diameter	181.8 mm
Tooth Tip Angle	27˚	Shaft Hole Diameter	0 mm
Sleeve thickness	0 mm	-	-

The axial dimensions describe the motor in terms of lengthwise i.e., running or extending in the direction of the length of the machine. Having obtained the stack length, the table below provides the various dimensions of the axial parameters of the motor.

Table 10 Axial Geometry for Stator and Rotor Parameters in the ANSYS MOTORCAD Software.

Axial Parameter	**Value**
Motor length	756.4 mm
Stator Lamination Length	412 mm
Magnet Length	402mm
Magnet Segment	1
Rotor Lamination Length	402mm

➢ *The Winding Input Tab*

The winding tab is utilized for describing the conductors and insulation located within the stator slots. The definition tab serves the purpose of outlining and visually representing the arrangement of conductors alongside insulation, impregnation, liner, and wedge. This facilitates the testing and examination of various winding setups. The pattern tab enables swift setup and visualization of the winding arrangement including coil connections, along with analysis of phasors, winding factors, and harmonic characteristics.

Table 11 Winding Tap Parameters for Both Definition and Pattern Tabs.

Definition Parameter	**Value**	**Pattern Parameter**	**Value**
Winding Type	Overlapping	Winding Type	Automatic
Winding Definition	Copper Slot Fill	Path Type	Central
Wedge Model	Wedge	Phases	3
Wire Diameter	1.247mm	Turns	11
Copper Diameter	1.171mm	Throw	5
Copper Slot Fill	0.45	Parallel Path	2
Liner Thickness	0.25mm	Winding Layers	Double Layer
Copper Depth	100%	-	-
Conductor Separation	0.02mm	-	-
Strands in hand	18	-	-

ISSN No:-2456-2165 https://doi.org/10.38124/ijisrt/26aug308

➢ *The Material Input Data*

This tab allows you to specify the various materials used in the construction of the generator.

The table below shows the various materials used for different components.

Table 12 Material for the Construction of the Various Components Used in ANSYS MOTOR CAD.

Components	**Material**
Stator Lamination Back Iron	Amon 7.3.25% Si
Stator Lamination Tooth	Amon 7.3.25% Si
Armature Winding	Copper(Pure)
Rotor Lamination Back Iron	Amon 7.3.25% Si
Magnet	N48H_AM
Shaft	Amon 7.3.25% Si

➢ *The Calculation Tab*

This allows us to set the operating conditions of the designed generator and run the finite element analysis of the generator. The table below presents a summary of the operating conditions used in performing the finite element simulation.

Table 13 A Summary of the Input Parameters Under the Calculation Tab in ANSYS Motor-CAD.

Parameter	**Value**
Shaft Speed	1500rpm
Line Current Definition	Peak
Peak Current	241A
DC Bus Voltage	614V
Phase Advance (Elect.Deg.)	45˚
Drive Type	Defined Current
Drive mode	Sine
Winding Connection	Delta Connection
Magnetization	Radial
Armature Winding Temperature	70˚C
Magnet Temperature	70˚C
E- Magnetics – Thermal Coupling	No Coupling
Skew	None

ISSN No:-2456-2165 https://doi.org/10.38124/ijisrt/26aug308

CHAPTER SEVRN
FINITE ELEMENT STUDY OF THE DESIGNED GENERATOR

➢ *Validation Results of the Designed Machine*

In this section, the results obtained from the finite element analysis, which was carried out using the ANSYS MOTOR CAD in both static open circuit and on-load conditions, are discussed. The discussion will include the presentation of the physical geometry of the designed generator as well as graphs showing variations of some important, designed parameters.

➢ *Presentation of the Designed Machine*

Following the completion of the simulation parameters of the generator in the ANSYS MOTOR CAD Software, Figure 13 below gives an idea of how the designed generator looks in a 3D geometry view. The total length of the designed generator is 756.4mm, but the stack length, which contributes to torque generation, is 412.6mm, while the external diameter is 451.10mm. However, in the real application of the design, the back-end shaft length will not be too long. Similarly, the front-end shaft length could also be reduced.

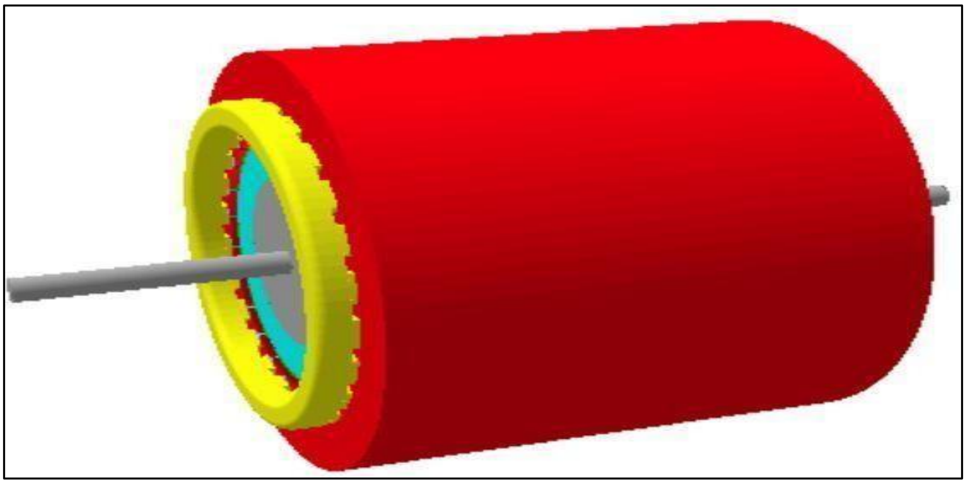

Fig 13 3D Axial View of the Designed Generator.

➢ *Flux Distribution in the Designed Generator*

Figure 14 below shows the flux distribution in the designed generator in static open circuit operation. One of the important considerations after finite element analysis is the flux distribution in the various parts of the machine. Flux saturation in any part of the core material can lead to a decrease in the efficiency of the machine since iron losses will increase. Again, it will lead to an increase in heat generation on that part of the machine. Additionally, saturation could lead to a distortion of the output signal that is voltage and current [18].

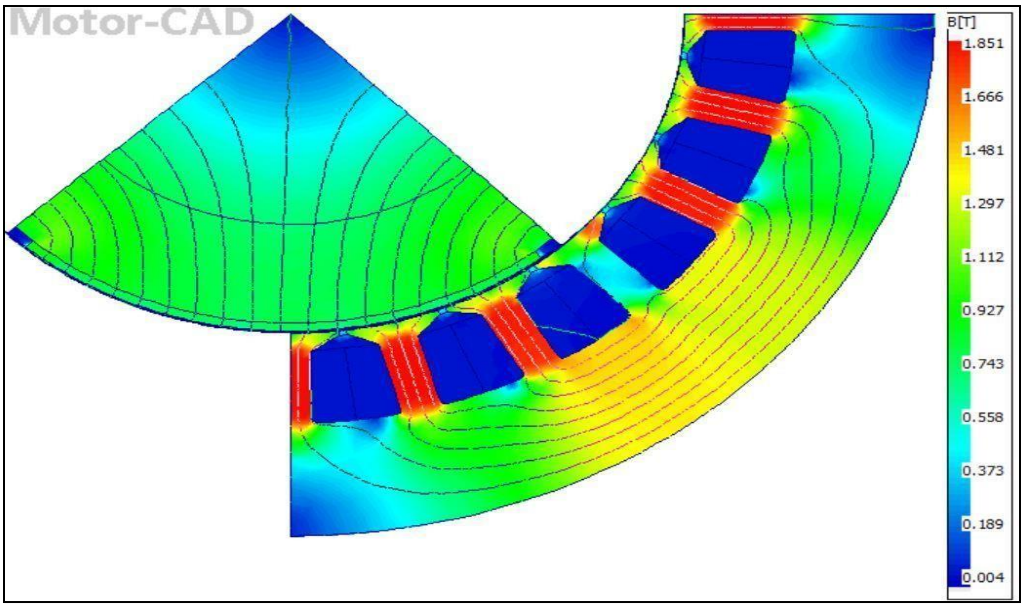

Fig 14 Flux Distribution in Various Parts of the Designed Machine.

ISSN No:-2456-2165 https://doi.org/10.38124/ijisrt/26aug308

In Figure 14 above, the flux density in the rotor back iron, the air gap, stator slots, stator tooth, and stator back iron are shown. The rectangular table gives an idea of the various flux densities in the parts mentioned. In the rotor back iron, the flux density is below 0.927T, and it nears zero towards the shaft. This is below the 1.6T taken in the analytical calculations. Additionally, the flux density in the stator tooth and tip is above 1.851T. This is above the

1.6T used in analytical calculations. Though the magnetic flux of the material is not enough to saturate at a current density of 30kA/m but to reduce the core losses and heat generated by the machine, the stator tooth width will be increased while monitoring a possible effect on the induced voltage and efficiency of the machine. In the stator back iron, the flux density is less than 1.222T, which is less than the 1.4T used in the analytical calculation. The graphs below show the variation between stator tooth width and peak flux density in the stator tooth.

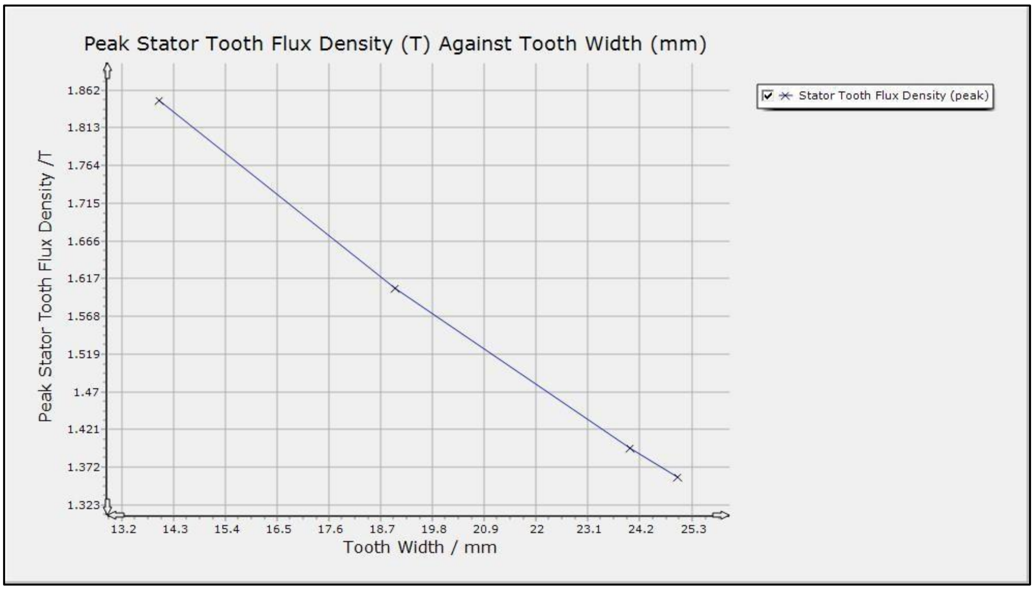

Fig 15 A Graph of Stator Tooth Peak Flux Density Against Tooth Width (mm).

From Figure 15, as the stator tooth width increases, the peak flux density in the stator tooth decreases. From this, if the flux density in the stator tooth should decrease, the width of the stator tooth must increase.

➢ *Cogging Torque Developed by the Designed Generator*

Considering a four-pole, twenty-four-slot, surface-mounted permanent magnet brushless machine, the cogging torque developed by the generator is analyzed.

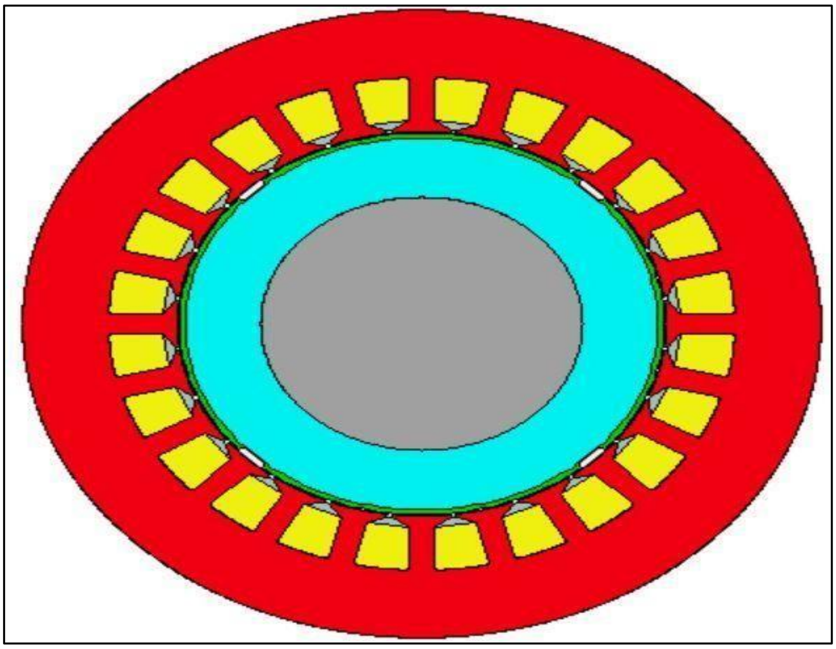

Fig 16 Cross Section of a Four Pole, Twenty-Four Slots, Surface Mounted Permanent Magnet Machine.

ISSN No:-2456-2165 https://doi.org/10.38124/ijisrt/26aug308

Below is a graphical presentation of the cogging torque developed by the designed machine. Cogging torque is an open circuit parameter which is an undesirable characteristic of a permanent magnet motor design.

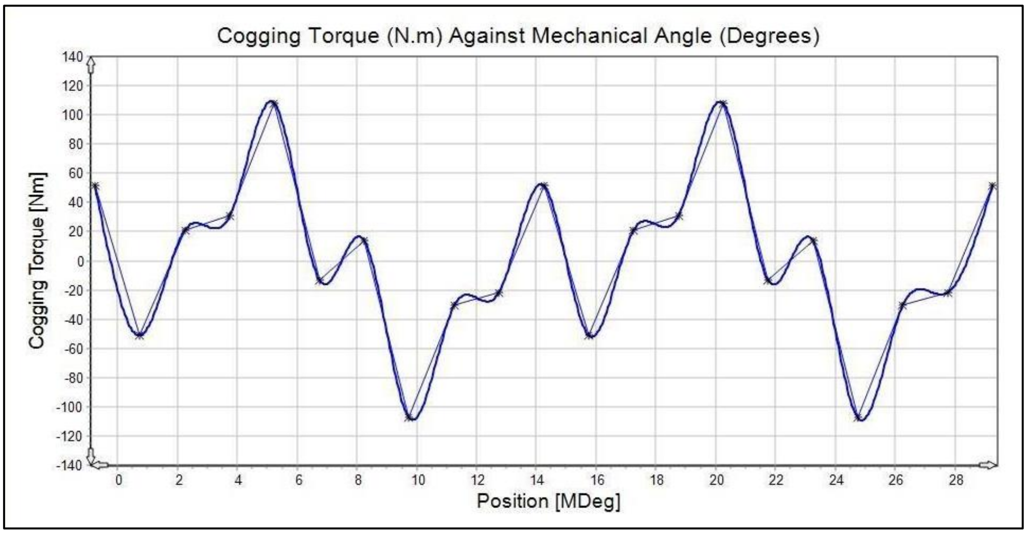

Fig 17 A Graph of Cogging Torque (N.m) Against Mechanical Angle (Degree)

It is generated when the sides of the rotor teeth line up with the sides of the stator teeth within the rotor. It is an undesired effect that contributes to the machine's output ripples, vibration, and noise[19]. In Figure 17 above, it is seen that at a rotor position of 4.5˚ the maximum cogging torque is recorded. It can then be concluded that the maximum cogging torque developed by the designed machine is 109.2N.m. What this means is that if the rotor should be assumed to rotate in an anticlockwise direction, it will reach a position in which the circumferential attractive forces will be maximum. In the other half cycle after maximum cogging torque, the rotor 'pulls' to a stable detent position. Any displacement of the rotor from this position results in cogging torque which attempts to re-align the rotor to this position. As the rotor rotates to complete one full cycle the cogging torque completes one cycle. During this rotation, the cogging torque is negative. This implies the circumferential components of attractive forces are attempting to prevent the rotor from rotating in the anticlockwise direction. Thus, the cogging torque is attempting to 'pull' the rotor back to its stable position. Many techniques such as variations in magnet strength, variations in magnet arc length, variations in the slot width, and permanent magnet skewing, have been found to reduce the effect of cogging torque [19]. For this reason, the original magnet arc electrical angle of 165˚and slot width of 14.30mm (slot and tooth width are the same) will be varied while monitoring any effect on the efficiency of the designed machine.

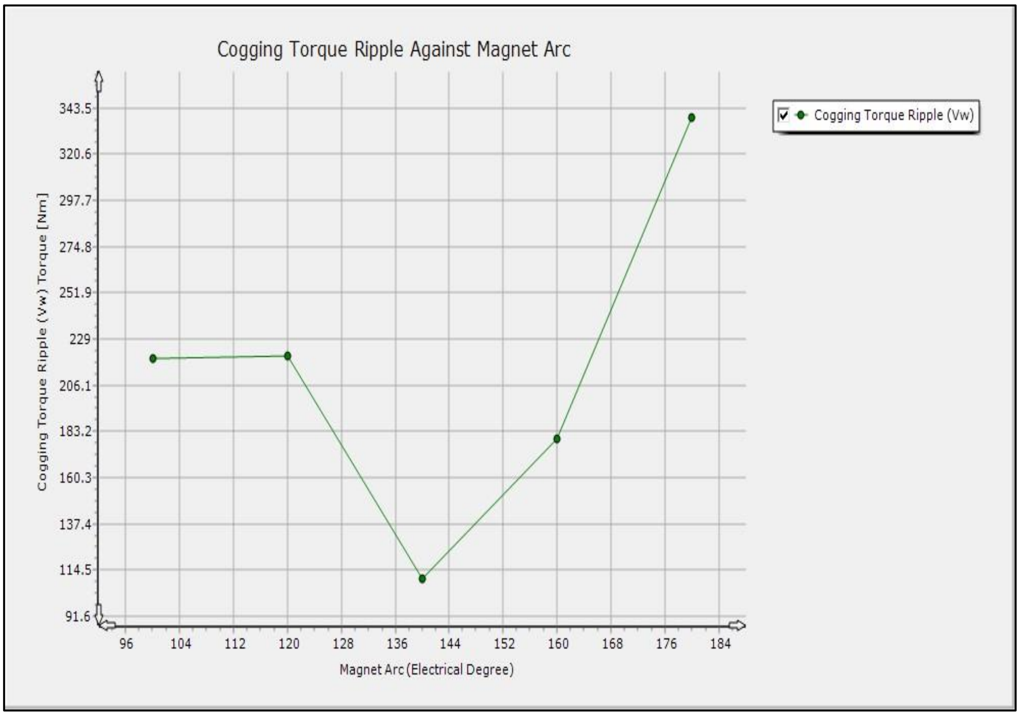

Fig 18 A Graph of Magnet Arc Against Cogging Torque Ripple.

ISSN No:-2456-2165 https://doi.org/10.38124/ijisrt/26aug308

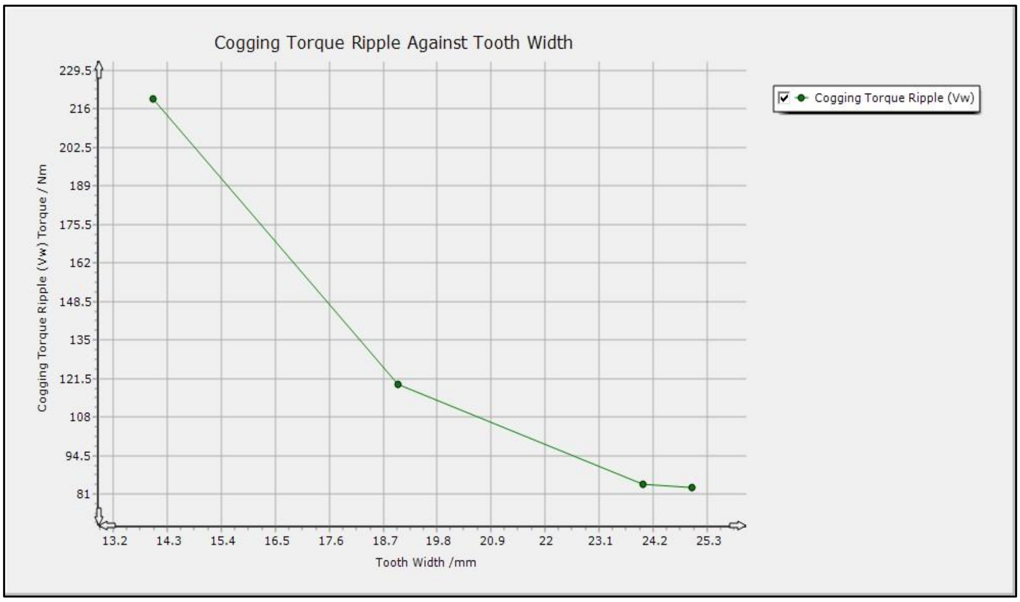

Fig 19 A Graph of Cogging Torque Ripple Against Tooth Width.

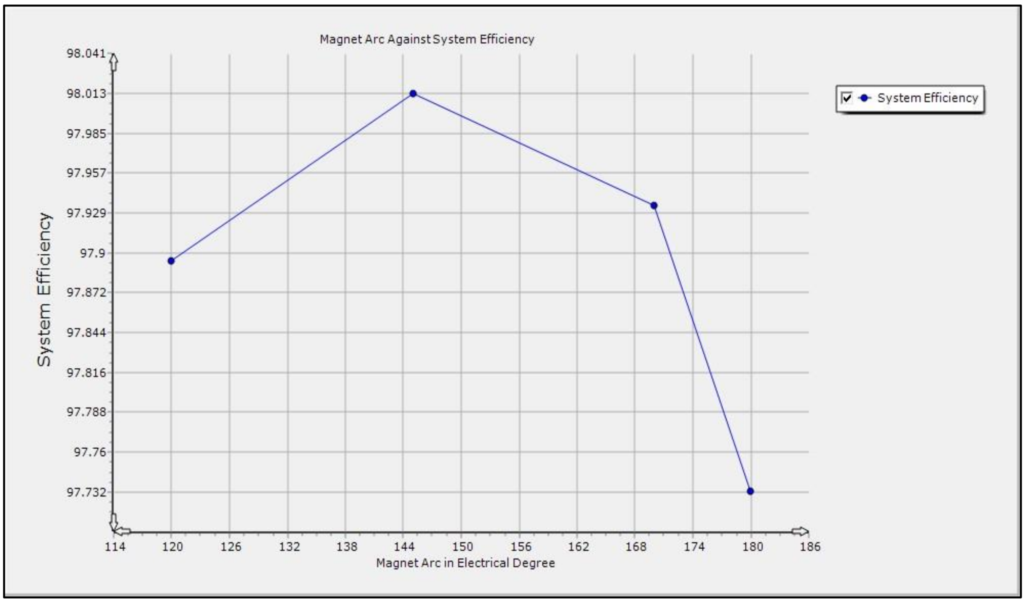

Fig 20 A Graph of System Efficiency Against Magnet Arc.

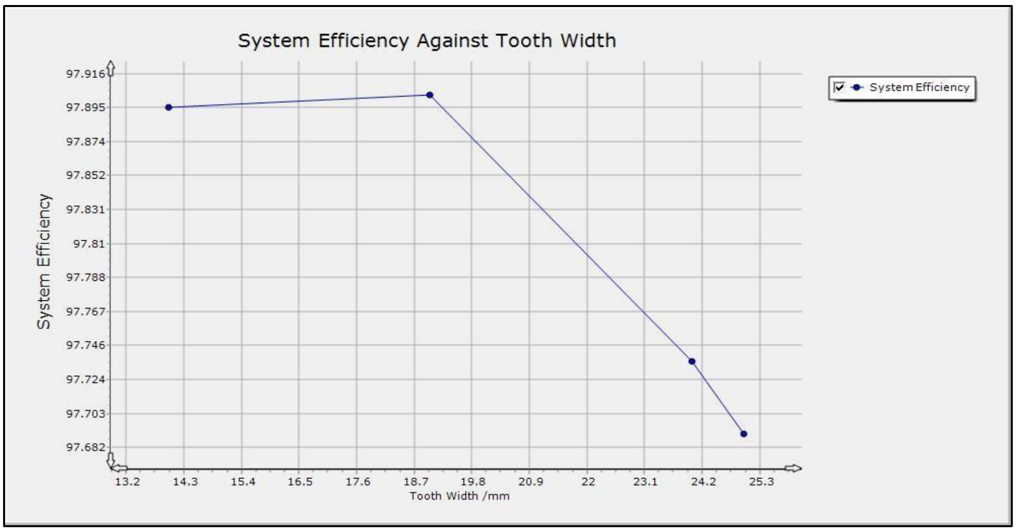

Fig 21 A Graph of System Efficiency Against Tooth Width.

ISSN No:-2456-2165 https://doi.org/10.38124/ijisrt/26aug308

In Figures 18 and 19 above, variations between cogging torque, magnet arc, and tooth width are investigated. In Figure 18, it is realized that as the magnet arc in electrical angle increases from 100˚ to 120˚ the cogging torque remains the same. On the other hand, between 120˚ to 140˚ the cogging torque saw a sharp decline with the lowest value recorded at 140 ̊. Increasing the magnet arc further above this angle, the cogging torque begins to increase. From the graph, it can therefore be concluded that for the machine to develop the lowest cogging torque, the magnet arc should be set at 140˚ electrical angles. Further to buttress this, it is seen in Figure 20 that as the magnet arc is set at 140˚ the efficiency of the machine is at optimum. Hence, the magnet arc of the designed machine will be set at 140 ̊. Additionally, in Figure 19, as the stator tooth width increases, the cogging torque developed by the machine decreases. This is to suggest that apart from changing the magnet arc, increasing the stator tooth width equally results in a further decrease in the cogging torque. However, the stator tooth width cannot be increased that much as its further increase results in the efficiency drop of the machine as demonstrated in Figure 21. For this reason, a balance should be made between increasing the stator tooth width, cogging torque, and efficiency. It is also noticed in Figure 13 that an increase in the stator tooth width results in a decrease in flux density in the tooth thereby preventing the tendency of saturation. Since the purpose of the design is to achieve the highest efficient generator for the wind turbine, the stator tooth width versus efficiency graph is used to determine the most appropriate stator tooth width. In Figure 21 above, the maximum efficiency is recorded when the stator tooth width is 19mm. Hence, instead of the initial 14.30mm used in the design, the stator tooth width will be set to 19mm.

➢ *Number of Turns and Induced Emf*

From the mathematical formula for calculating the induced emf, the induced emf is directly proportional to the number of turns per phase. The voltage at the terminal of the generator when connected to the load also depends on the induced voltage and the voltage drop across the armature windings. Since power is supplied to the factory at a phase voltage of 433V and the proposed generator is delta-connected, the required voltage at the terminals at rated conditions is expected to be 433V. For this reason, the number of turns varies over different numbers of turns while monitoring the induced voltage and the terminal voltage. This was carried out in the sensitivity analysis tab of the ANSYS MOTOR CAD Software. The graph below shows the variation between the number of turns and the line-line voltage.

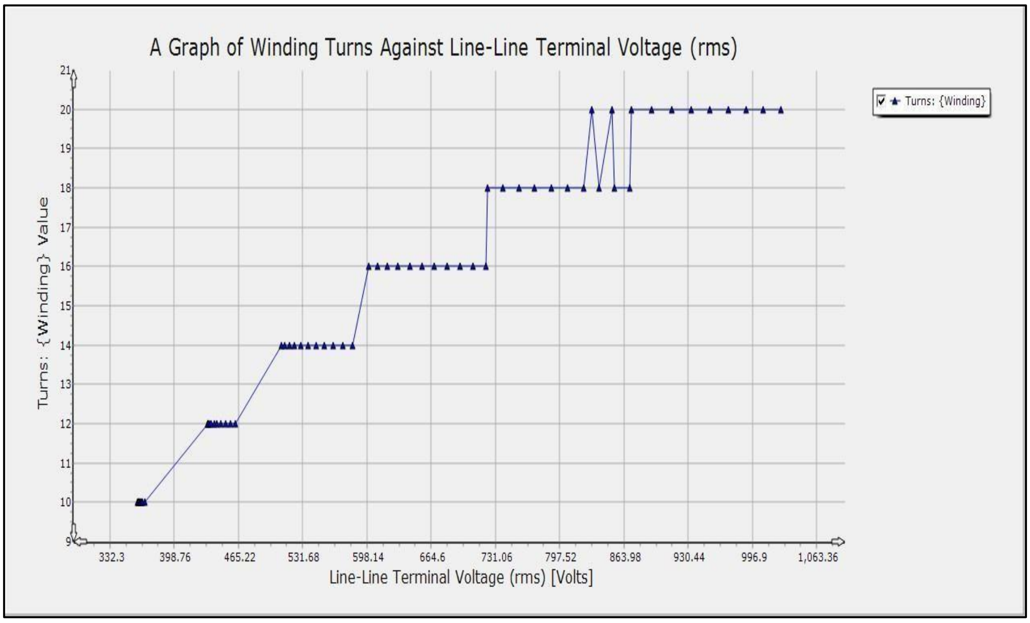

Fig 22 A Graph Showing the Variation Between the Number of Turns and Line - Line Voltage.

In Figure 22 above, to be able to achieve a terminal voltage of 433V at rated conditions when the generator is connected to a load, the number of turns must increase to 12 instead of the 11 initially used. However, increasing the number of turns increases the I^2R losses, which in turn affects the efficiency of the machine but in this case, efficiency does not see any substantial change. Hence, the proposed generator will have 12 turns.

➢ *Torque and Peak Load Current*

The designed generator will supply load current at a frequency of 50Hz. This frequency is maintained by balancing the electrical load powers Pe with the generator input mechanical powers Pm. The total applied torque is due to the input mechanical torque on the rotor shaft, which is provided by the turbine, and the output mechanical torque from the electrical load i.e., a reaction torque on the rotor windings [20]. So, the input torque must be equal to the electrical load torque. However, the electrical load torque is dependent on the load current. Hence, the initial peak load current of 241A, which was expected from the generator, will be varied while monitoring the mechanical shaft torque to be 904.12N · m as calculated at rated conditions. This was carried out in the sensitivity analysis tab of the ANSYS MOTOR CAD Software by varying the peak load current over several iterations. The graph below shows the variation of the mechanical torque input and peak load current.

ISSN No:-2456-2165 https://doi.org/10.38124/ijisrt/26aug308

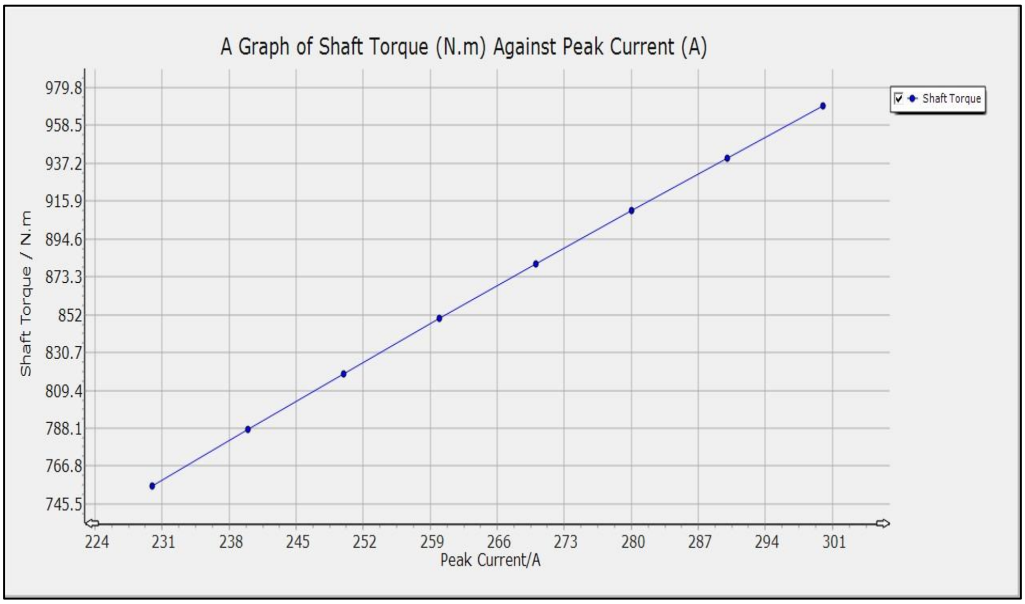

Fig 23 A Graph of Mechanical Shaft Torque (N.m) Against Peak Load Current (A)

In Figure 23 above, it is seen that as the peak load current increases, the mechanical torque generated by the rotor shaft also increases. At a peak current of 281A, the mechanical torque is observed to be 904.55N · m, which is equivalent to the mechanical torque produced by the turbine at rated conditions. In doing this, the efficiency of the designed generator is monitored since increasing the load current will lead to an increase in the I^2R losses in the armature windings. Since the efficiency did not show any substantial difference, the peak load current of the design generator is taken as 281A.

- *Effect of Magnet Size on Induced Voltage*

The voltage induced in the armature windings depends on the strength of the magnetic field, the speed of the rotation, and the number of turns. In this section, the effect of magnet size on terminal voltage is investigated. Since the field excitation is from a permanent magnet, the strength of the magnetic field will also depend on the size of the magnet, which corresponds to how much voltage is induced in the armature winding. The graph below shows a variation between magnet size and terminal voltage.

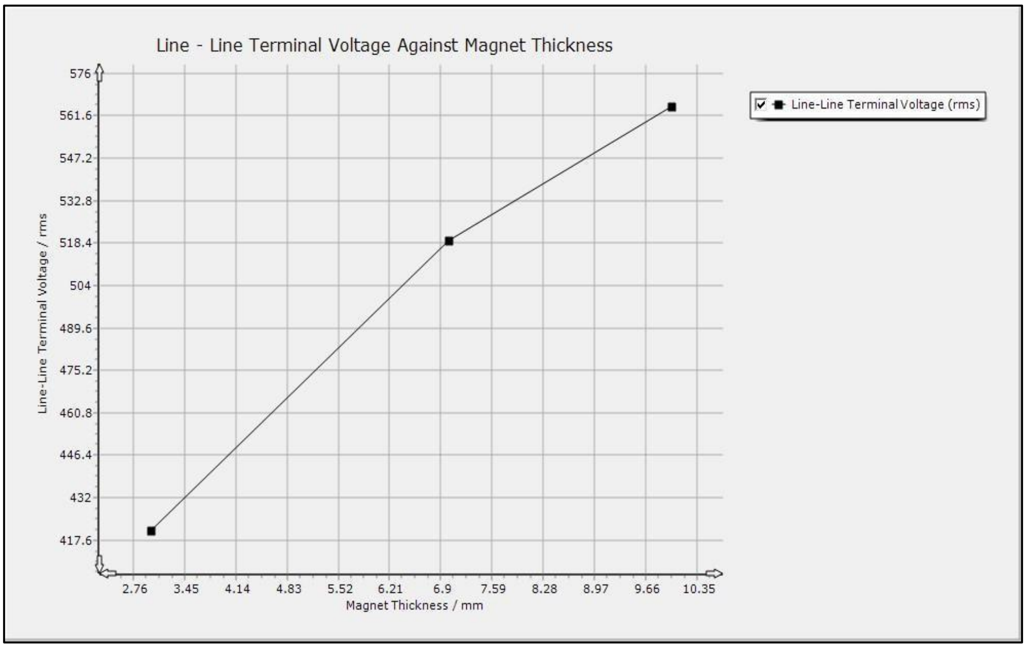

Fig 24 A Graph of Line -Line Terminal Voltage Against Magnet Thickness.

In Figure 24 above, as the magnet thickness increases, the terminal voltage also increases. It is key to mention that the terminal voltage depends on the induced voltage, so if the terminal voltage is increasing, then the induced voltage is also increasing. There is a limit to the voltage required at the terminal of the generator when connected to a load. Hence, from Figure 24 above, it is appropriate to keep the magnet thickness at 3.58mm since the terminal voltage is exactly 433V as required.

ISSN No:-2456-2165 https://doi.org/10.38124/ijisrt/26aug308

➢ *Summary of Changes Made to Initial Design Parameters*

As discussed above, a few parameters have been changed to improve the performance and efficiency of the machine design. To proceed with other performance indicators, these design changes are made in the ANSYS MOTOR CAD Software. The table below gives a summary of the design parameters changed.

Table 14 A Summary of the Design Changes Made to the Original Parameters.

Parameter	Initial Value	Final Value
Magnet Arc	165˚	140˚
Stator Tooth Width	14.30mm	19mm
Number of Turns per Coil	11	12
Peak Line Current	241A	281A

➢ *The Output Graphs of the Generator*

Following the implementation of the design changes above, the various outputs and other parameters of the designed generator are presented below.

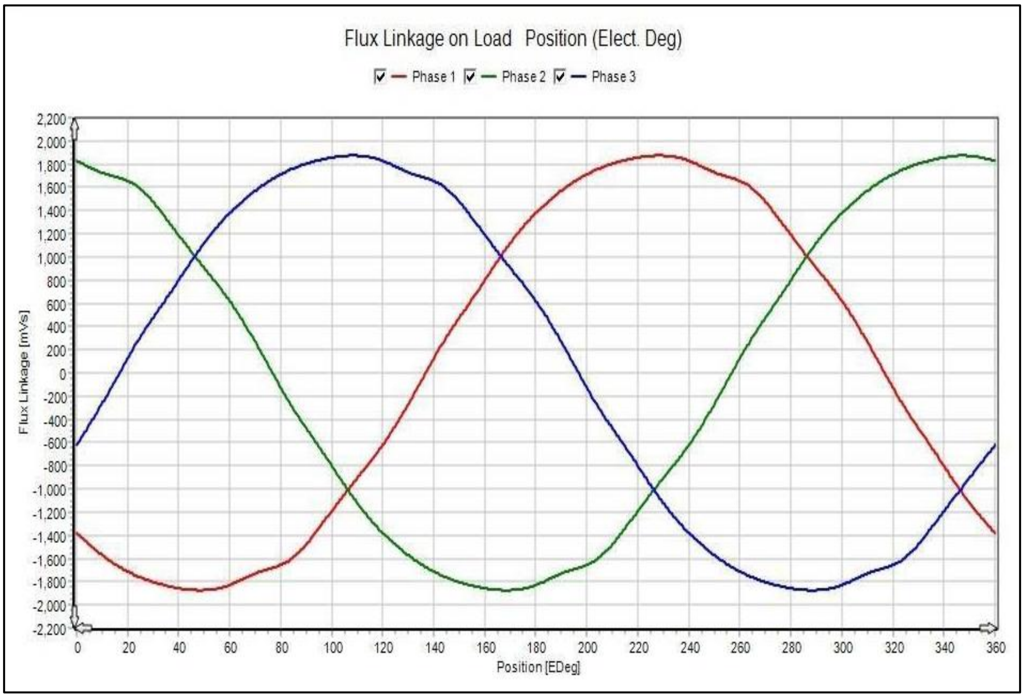

Fig 25 A Graph of Flux Linkage Against Position of Rotor in Electrical Angle.

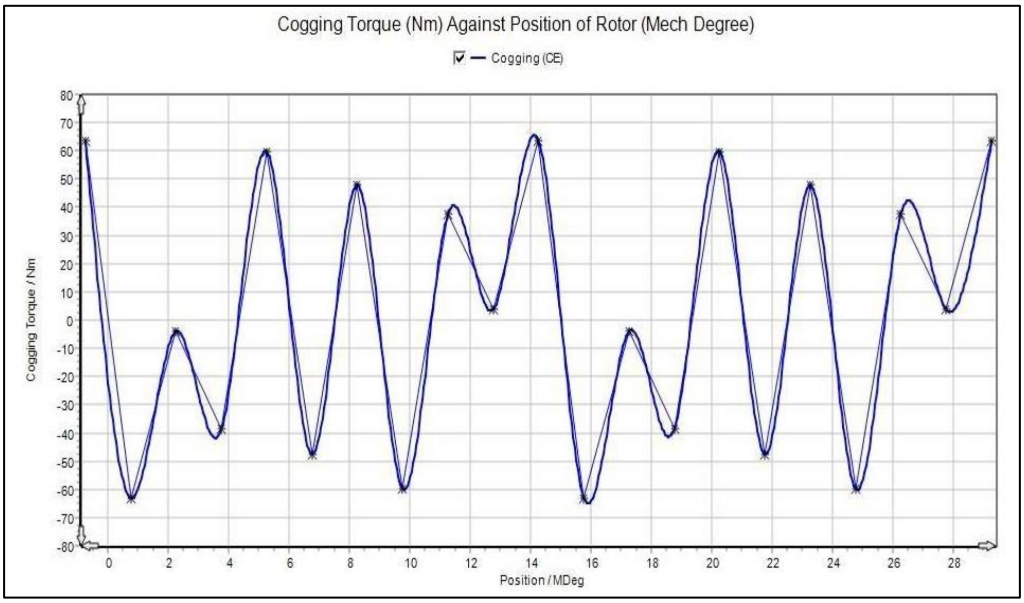

Fig 26 Final Machine Cogging Torque Against Position of Rotor in Mechanical Angle.

ISSN No:-2456-2165 https://doi.org/10.38124/ijisrt/26aug308

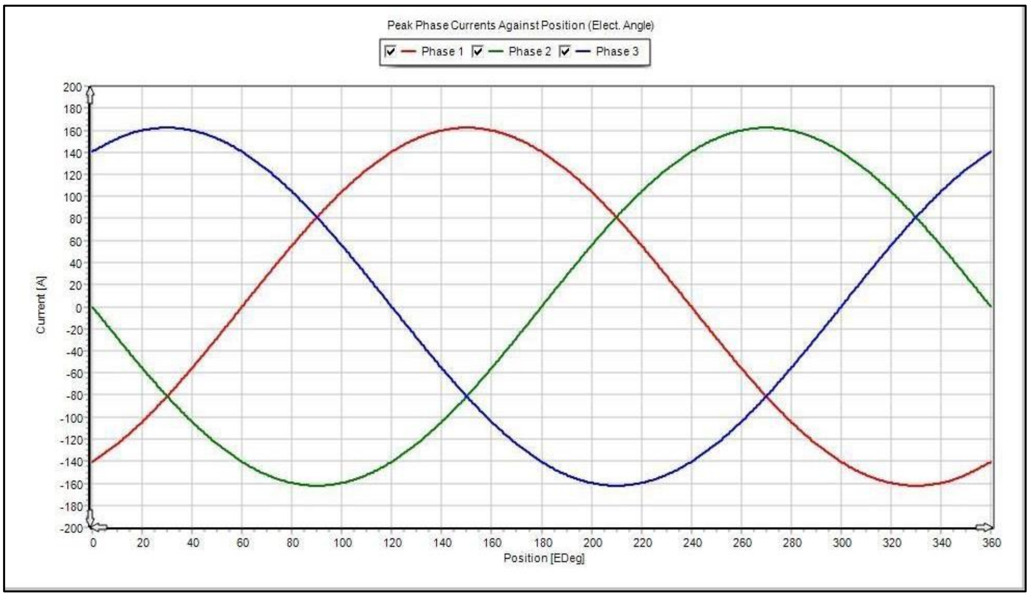

Fig 27 A Graph of Peak Phase Current Against Rotor Position in Electrical Angle.

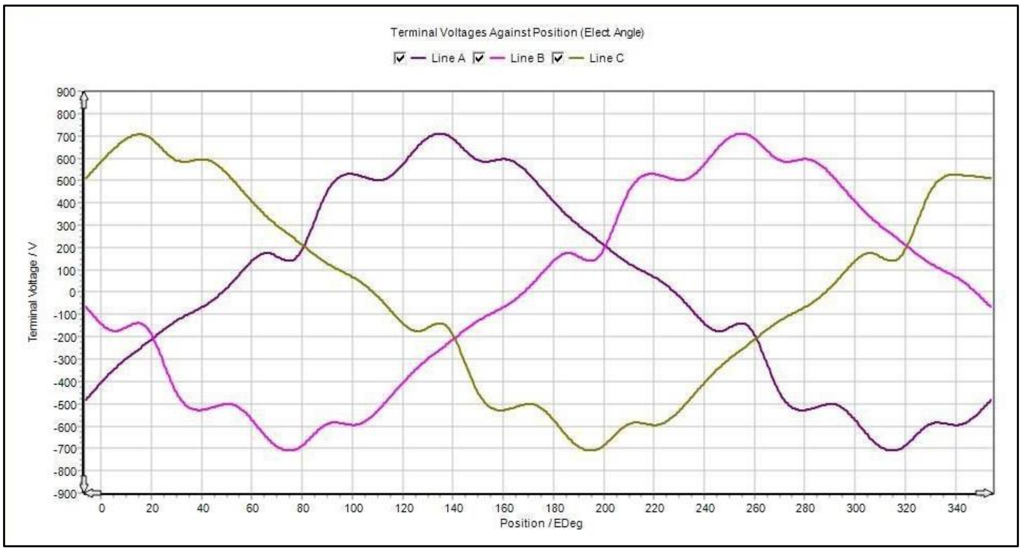

Fig 28 A Graph of Terminal Voltages Against Rotor Position in Electrical Angle.

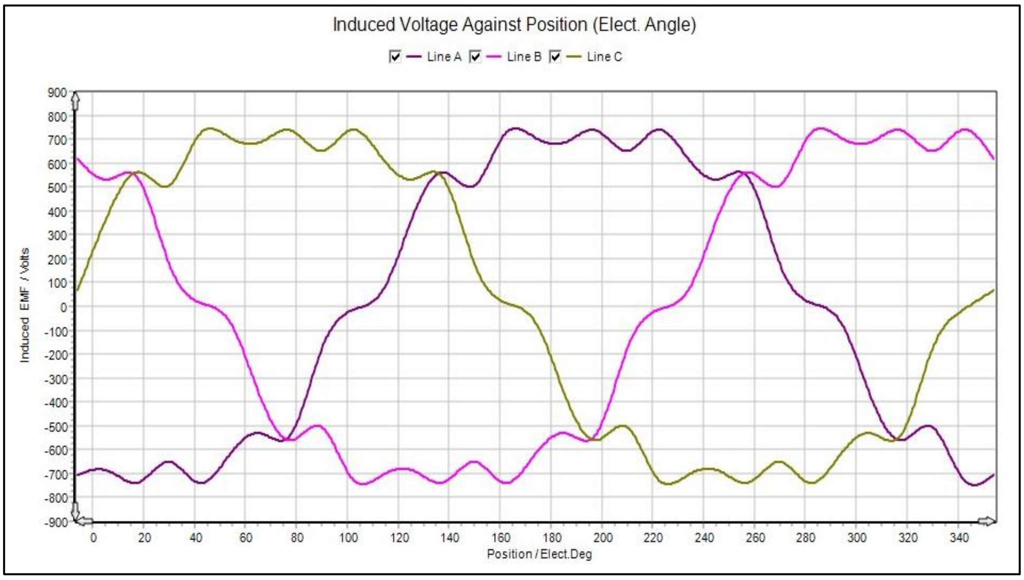

Fig 29 A Graph of Induced Voltage Against Rotor Position in Electrical Angle.

ISSN No:-2456-2165 https://doi.org/10.38124/ijisrt/26aug308

Figure 25 depicted above illustrates a flux linkage waveform characterized by a wellformed sinusoidal shape. This implies that the magnetic field remains non–saturated even under substantial excitation levels. Consequently, there should be no distortion present in the electromotive force (EMF) waveform as it crosses the zero point. Additionally, the closely matched amplitudes of the flux linkage for phases 1, 2, and 3 can be attributed to the minimal occurrence of the fringing effect. Figure 26 shows the cogging torque developed by the machine following some changes made in the initial parameters. The peak cogging torque of the machine is 65 N · m. In Figure 27, the phase sinusoidal terminal voltage is presented. This is expected to be the voltage across the terminal of the generator when connected to a load. The peak terminal voltage is 702V, which has some 13% harmonic distortion. Figure 28 represents a three-phase sinusoidal induced voltage with a peak value of 740V. Figure 29 shows the phase current of the designed generator if connected to a load. The peak phase current is noticed to be 162A (Delta Connection).

ISSN No:-2456-2165 https://doi.org/10.38124/ijisrt/26aug308

CHAPTER EIGHT
PERFORMANCE SENSITIVITY ANALYSIS OF THE DESIGNED MACHINE

➢ *Performance Testing of the Designed Generator*

The performance of the designed generator is evaluated under different rotor speeds. Since it is a wind turbine, the speed of the rotor is expected to change with time. The graphs below are used to analyze the generator's performance.

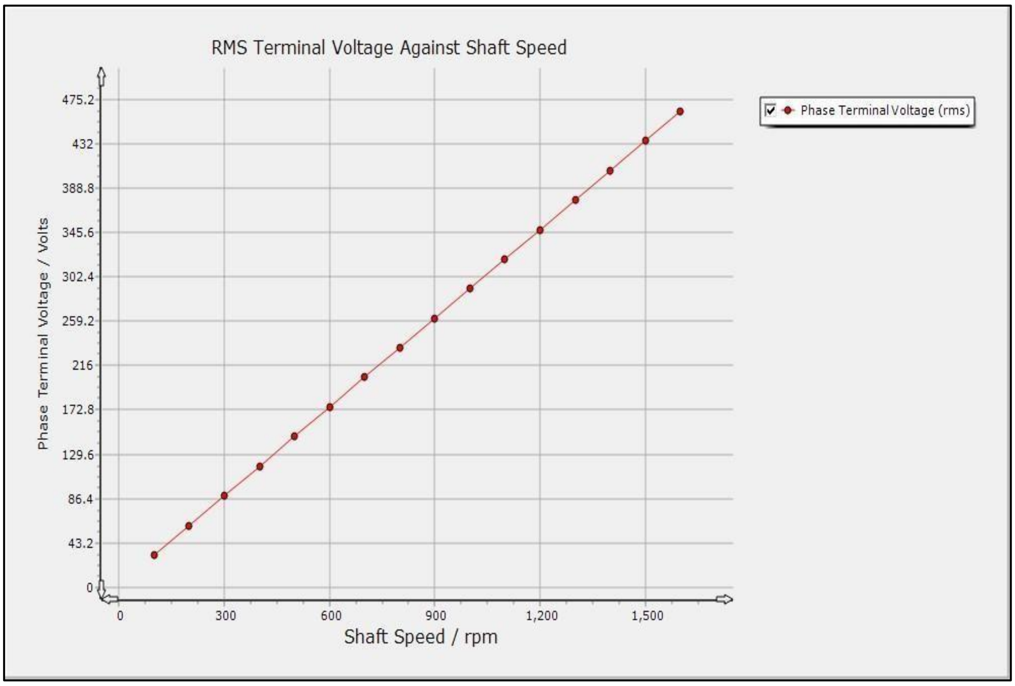

Fig 30 Graph of RMS Terminal Voltage Against Shaft Speed.

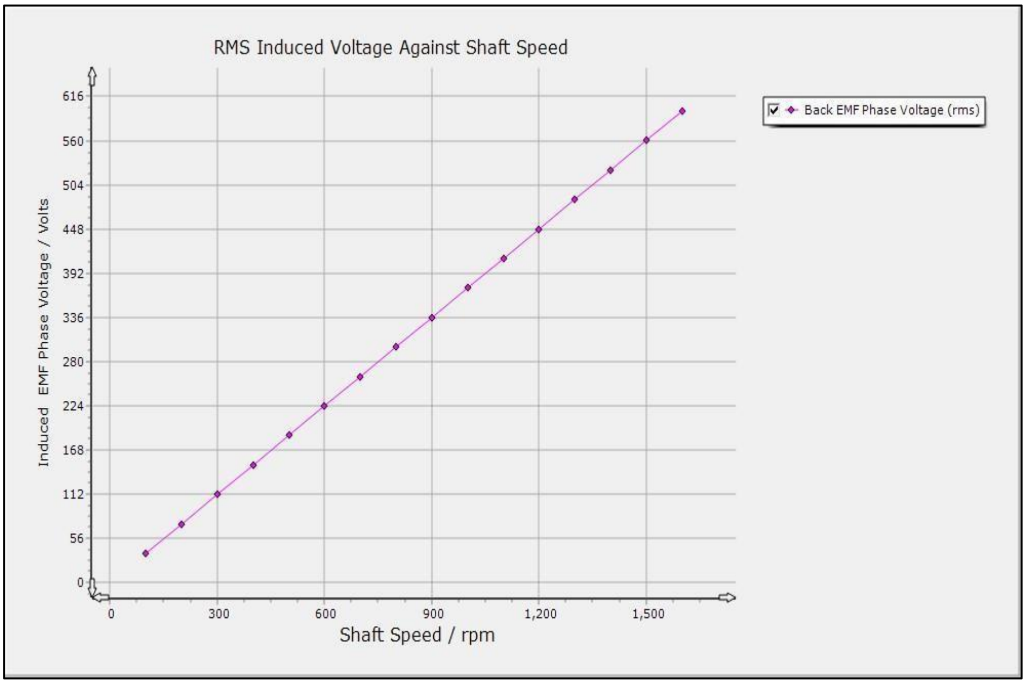

Fig 31 A Graph of RMS Induced Emf Against Shaft Speed.

Fig 32 A Graph of System Efficiency Against Shaft Speed

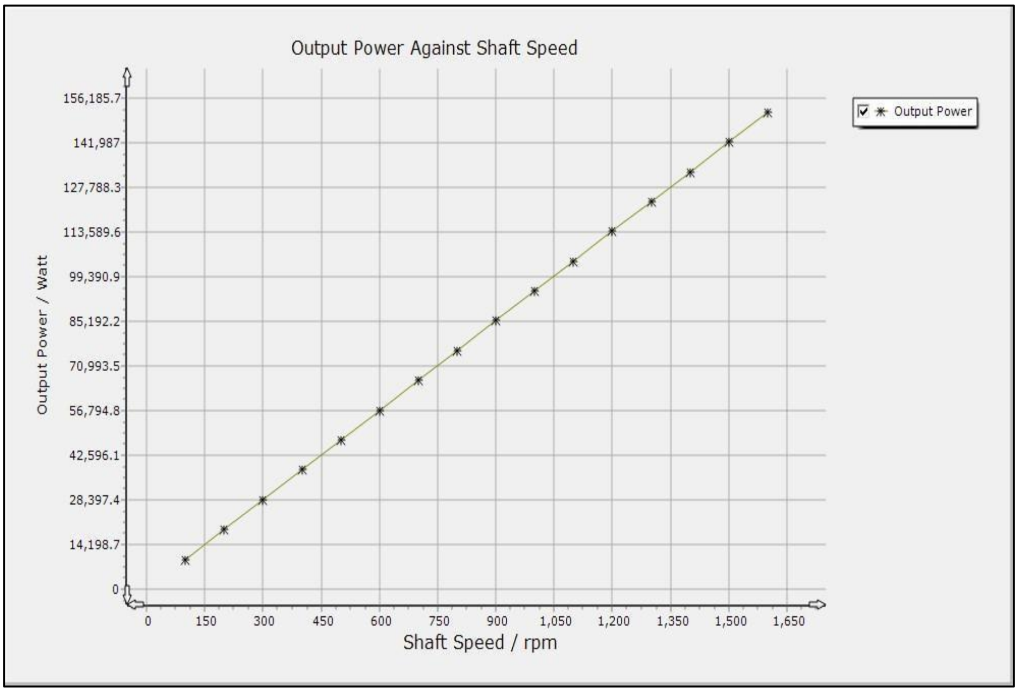

Fig 33 A Graph of Output Power Against Shaft Speed

Figure 30 above shows the generator's performance when connected to a load. It depicts what the terminal voltage of the generator will be should the rotating speed of the rotor change with time. Under-rated conditions, when the rotor speed is 1500rpm the terminal voltage is 435V. Similarly, Figure 31 shows the dependency of induced voltage on the speed of rotation of the excitation field. It is seen that as the speed of rotation increases, the RMS Induced voltage also increases. At rated conditions, when the rotor is spinning at 1500 rpm, the induced voltage is 560.2V. Figure 32 talks about the performance of the generator at varying speeds. Since a varying speed changes the generator's terminal voltage, which characterizes the output power of the generator, it suggests that at a varying speed, the efficiency of the machine will change. At the rated condition of 1500rpm of the rotor, the machine will be 98.52% efficient. Lastly, in Figure 33, the output electrical power of the designed generator is shown. It can be concluded that at a rated rotor speed of 1500rpm, the designed generator can deliver 142kW power.

➢ *Thermal Analysis*

The housing of the generator is designed and the thermal performance of the generator at a transient state is analyzed at an ambient temperature of 25˚C as shown in the figure below.

ISSN No:-2456-2165 https://doi.org/10.38124/ijisrt/26aug308

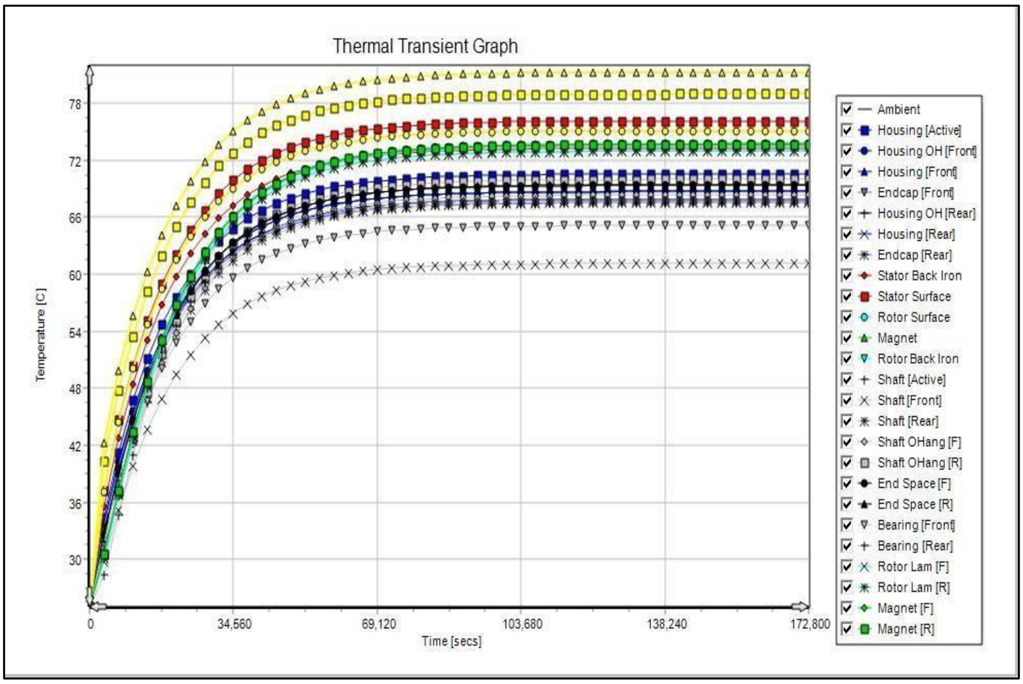

Fig 34 A Graph of Temperature Against Time for Designed Machine.

In Figure 34 above, the temperature that will be developed by the machine if it continuously works for 2 days is simulated to obtain the maximum operating temperature. The temperature developed by all parts of the machine is obtained in the graph above. One essential part is the temperature developed on the magnet. It is known that magnets have curie temperatures, and temperatures above their curie point will render the magnet demagnetized. From the graph, as the machine operates to attain a steady state the temperature developed on the magnet is 73.7˚C which is less than the curie temperature of Neodymium Iron Boron magnet. The highest temperature is developed in the machine windings which is recorded as 81.3˚C. Hence, the maximum operating temperature of the generator can be said to be 81.3˚C and therefore does not require active cooling methodologies.

➢ *Comparison Between Performance Parameters of the Analytical and Validated Design*

The table below compares the performance parameters of the analytical calculations and simulated deigned of the wind turbine generator.

Table 15 Performance Parameter for Analytical and Simulated Design for the Wind Turbine Generator.

Performance Parameter	Designed	Simulated	Check
Output Power	115.036kW	142kW	Acceptable
Input torque	904.1255Nm	904.55Nm	Delivered
Terminal Voltage (rms)	433V	435V	Delivered
Induces EMF (rms)	482.0523V	560.2V	Above
Efficiency	98.57%	98.52%	Delivered
Peak Line Current	241A	281A	Delivered
Operating Temperature	70˚C	81.3˚C	Acceptable

ISSN No:-2456-2165 https://doi.org/10.38124/ijisrt/26aug308

CHAPTER NINE
CONCLUSION

An analytical technique was introduced for designing a high-efficiency surface permanent magnet synchronous generator. This method allows for obtaining the machinery's magnet thickness and dimension of all parts of the machine. The impact of magnetic flux density on various dimensions of the machine was analyzed. A successful design was accomplished for a 142kW, 1500rpm surface-mounted permanent magnet generator with 24 slots and 4 pole topologies. This design was thoroughly optimized and validated using ANSYS MOTOR CAD SOFTWARE analysis based on finite element methodology. The housing design was created, and thermal performance analysis was conducted for each generator component. Notably, the generator exhibited excellent heat dissipation without the need for an additional fan. Simulation and testing outcomes verified that the generator's key features and performance criteria were met. In the future., research on this generator application will concentrate on developing a sensor-less control system. Additionally, a three-phase active rectifier will be designed to acquire DC bus voltage from the generator's three-phase outputs.

ISSN No:-2456-2165 https://doi.org/10.38124/ijisrt/26aug308

REFERENCES

[1]. ANTÓNIO GUTERRES, "Causes and Effects of Climate Change | United Nations," *United Nations Publications,* Jun. 23, 2023. https://www.un.org/en/climatechange/science/causes-effects-climate-change (accessed Jun. 12, 2023).

[2]. Ines Gendre, "What is global warming?," *The Climate Expert's Blog* , Sep. 29, 2022. https://greenly.earth/en-us/blog/ecology-news/what-is-global-warming? (accessed Jun. 12, 2023).

[3]. Nexamp, "Solar Vs. Wind Energy," *Nexamp Blog Publication,* Jan. 15, 2021. https://www.nexamp.com/blog/solar-power-vs-wind-energy (accessed Jun. 13, 2023).

[4]. "Wind Turbine: The Need For Permanent Magnet | Borates Today," *Borates Today Limited*, Sep. 18, 2021. https://borates.today/wind-turbine-need-for-permanent- magnet/ (accessed Aug. 31, 2023).

[5]. Ruth Barrientos Díaz, "We discover the founding precursors of wind power | Siemens Gamesa | International inventors' day," *Siemens Gamesa Renewable Energy*, Nov. 08, 2019. https://www.siemensgamesa.com/explore/journal/2019/11/siemens-gamesa- inventors-day (accessed Jun. 07, 2023).

[6]. P. Gipe and E. Möllerström, "An overview of the history of wind turbine development: Part I—The early wind turbines until the 1960s," *Wind Engineering*, vol. 46, no. 6. SAGE Publications Inc., pp. 1973–2004, Dec. 01, 2022. doi: 10.1177/0309524X221117825.

[7]. G. Suresh, M. Raju, S. Kumar Tiwari, D. Sundeep, and S. Javid Pasha, "DESIGN AND ANALYSIS OF A VERTICAL AXIS WIND TURBINE BLADE." Accessed: Aug. 31, 2023. [Online]. Available: c

[8]. JOHN MARTIN GILL, "The Parts of a Wind Turbine: Major Components Explained - Energy Follower," *Energy Follower Publication*, Nov. 10, 2021. https://energyfollower.com/parts-of-a-wind-turbine/ (accessed Jun. 07, 2023).

[9]. N. S. Çetin, M. A. Yurdusev, R. Ata, and A. Özdemir, "Assessment of optimum tip speed ratio of wind turbines," *Mathematical and Computational Applications*, vol. 10, no. 1, pp. 147–154, 2005, doi: 10.3390/mca10010147.

[10]. W. Cao, Y. Xie, Z. Tan, W. Cao, Y. Xie, and Z. Tan, "Wind Turbine Generator Technologies," *Advances in Wind Power*, Nov. 2012, doi: 10.5772/51780.

[11]. B. Hoen *et al.*, "Attitudes of U.S. Wind Turbine Neighbors: Analysis of a Nationwide Survey," *Energy Policy*, vol. 134, Nov. 2019, doi: 10.1016/j.enpol.2019.110981.

[12]. R. S. Ehrmann, B. Wilcox, E. B. White, D. C. Maniaci, and S. Technical Manager, "SANDIA REPORT Effect of Surface Roughness on Wind Turbine Performance," 2017. [Online]. Available: http://www.ntis.gov/help/ordermethods.asp?loc=7-40#online

[13]. X. Zhang, J. Jia, L. Zheng, W. Yi, and Z. Zhang, "Maximum power point tracking algorithms for wind power generation system: Review, comparison and analysis," *Energy Sci Eng*, vol. 11, no. 1, pp. 430–444, Jan. 2023, doi: 10.1002/ESE3.1313.

[14]. N. H. Rivani and R. Elson, "Design and Analysis of Permanent Magnet Synchronous Generator 12 Slots 8 Poles for Small Scale Wind Turbine."

[15]. J. E. Rucker, "Calhoun: The NPS Institutional Archive Design and analysis of a permanent magnet generator for naval applications," 2005. [Online]. Available: http://hdl.handle.net/10945/11053

[16]. J. R. Hendershot and T. Miller, "DESIGN OF BRUSHLESS PERMANENTMAGNET MOTORS."

[17]. J. Pyrhönen, T. Jokinen, V. Hrabovcová, and H. Niemelä, "DESIGN OF ROTATING ELECTRICAL MACHINES."

[18]. "Understanding Magnetic Saturation and Its Effects | Electrical4U," *https://www.electrical4u.com/*, May 2023, Accessed: Aug. 10, 2023. [Online]. Available: https://www.electrical4u.com/magnetic-saturation/

[19]. C. Studer, S. A. Member Keyhani, T. Sebastian, and M. S. K Murthy, "Study of Cogging Torque in Permanent Magnet Machines."

[20]. Professor David Thomas, "POWER SYSTEM CONTROL AND STABILITY," Nottingham.